19. Takeuchi H, Kobayashi Y, Ishigaki S, Doyu M, Sobue G. Mitochondrial localization of mutant superoxide dismutase 1 triggers caspase-dependent cell death in a cellular model of familial amyotrophic lateral sclerosis. *J Biol Chem* 2002; **277**: 50966–50972.
20. Kang SJ, Sanchez I, Jing N, Yuan J. Dissociation between neurodegeneration and caspase-11-mediated activation of caspase-1 and caspase-3 in a mouse model of amyotrophic lateral sclerosis. *J Neurosci* 2003; **23**: 5455–5460.
21. Krajewska M, Wang HG, Krajewski S *et al.* Immunohistochemical analysis of in vivo patterns of expression of CPP32 (Caspase-3), a cell death protease. *Cancer Res* 1997; **57**: 1605–1613.
22. Inoue H, Tsukita K, Iwasato T *et al.* The crucial role of caspase-9 in the disease progression of a transgenic ALS mouse model. *EMBO J* 2003; **22**: 6665–6674.
23. Kaasik A, Vassiljev V, Poldoja E, Kalda A, Zharkovsky A. Do nuclear condensation or fragmentation and DNA fragmentation reflect the mode of neuronal death? *Neuroreport* 1999; **10**: 1937–1942.
24. Matter A. Microcinematographic and electron microscopic analysis of target cell lysis induced by cytotoxic T lymphocytes. *Immunology* 1979; **36**: 179–190.
25. Bursch W, Paffe S, Putz B, Barthel G, Schulte-Hermann R. Determination of the length of the histological stages of apoptosis in normal liver and in altered hepatic foci of rats. *Carcinogenesis* 1990; **11**: 847–853.
26. Kihira T, Yoshida S, Hironishi M, Wakayama I, Yase Y. Neuronal degeneration in amyotrophic lateral sclerosis is mediated by a possible mechanism different from classical apoptosis. *Neuropathology* 1998; **18**: 301–308.
27. Migheli A, Aztori C, Piva R *et al.* Lack of apoptosis in mice with ALS. *Nature Med* 1999; **5**: 966–967.
28. He BP, Strong MJ. Motor neuronal death in sporadic amyotrophic lateral sclerosis (ALS) is not apoptotic. A comparative study of ALS and chronic aluminum chloride neurotoxicity in New Zealand white rabbits. *Neuropathol Appl Neurobiol* 2000; **26**: 150–160.

J Neuropathol Exp Neurol


Vol. 64, No. 8
August 2005
pp. 665–674

ORIGINAL ARTICLE

# Visualization of Newly Deposited tau in Neurofibrillary Tangles and Neuropil Threads

Tomohiro Miyasaka, PhD, Atsushi Watanabe, PhD, Yuko Saito, MD, Shigeo Murayama, MD, David M. A. Mann, PhD, Mineo Yamazaki, MD, Rivka Ravid, PhD, Maho Morishima-Kawashima, PhD, Kazuo Nagashima, MD, and Yasuo Ihara, MD

**Abstract**

Neurofibrillary tangles (NFTs) and neuropil threads (NTs), the major hallmark of Alzheimer disease (AD), are composed of the microtubule-associated protein tau that has undergone posttranslational modifications, including deamidation and isomerization on asparaginyl or aspartyl residues. Because such modifications represent protein aging, we generated 2 antibodies, TM4, specific for Asp-387 of tau, and iD387, specific for isoAsp-387 of tau, to investigate the evolution of NFTs and NTs. On Western blots of Sarkosyl-insoluble fractions, TM4 strongly labeled paired helical filament-tau (PHF-tau), whereas iD387 preferentially labeled PHF smear. Thus, it is reasonable to postulate that TM4-labeled tau (unmodified tau species) represents more recent deposition, and iD387-labeled tau (modified tau species) represents earlier deposition. Unexpectedly, TM4 immunostained even highly evolved NFTs, suggesting that deposition of newly produced tau continues until neuronal death. iD387 labeled the whole profile of NFTs up to distal dendritic branches, whereas TM4 staining was localized to particular portions of NFTs in proximal dendrites and neuronal perikarya. In NTs, TM4 preferentially labeled the outer portion, whereas iD387 intensely labeled the core portion. Based on TM4-positive NFT counts and total NFT counts, we speculate that NFTs in the human hippocampus are produced at a constant rate irrespective of the disease stage.

From the Department of Neuropathology (TM, MMK, YI), Faculty of Medicine, University of Tokyo, Tokyo, Japan; Laboratory of Molecular and Cellular Pathology (TM, KN), School of Medicine, Hokkaido University, Sapporo, Japan; Biomolecular Characterization Division (AW), Characterization Center, RIKEN (The Institute of Physical and Chemical Research), Japan; Department of Neuropathology (YS, SM), Tokyo Metropolitan Institute of Gerontology, Japan; Department of Medicine (DMAM), University of Manchester, Manchester, United Kingdom; Department of Neurology (MY), Nippon Medical School, Japan; The Netherlands Brain Bank (RR), Amsterdam, The Netherlands; and the Core Research for Evolutional Science and Technology (CREST) (YI), Japan Science and Technology Corporation (JST), Kawaguchi, Japan.

Send correspondence and reprint requests to: Yasuo Ihara, MD, Department of Neuropathology, Faculty of Medicine, University of Tokyo, 7-3-1 Hongo, Bunkyo-ku, Tokyo 113-0033, Japan; E-mail: yihara@m.u-tokyo.ac.jp

This work was supported in part by a Grant-in-Aid for Scientific Research on Priority Areas—Advanced Brain Science Project—from Ministry of Education, Culture, Sports, and Science and Technology, Japan (YI); and by a Research Grant for Longevity Sciences from the Ministry of Health and Welfare, Japan (MMK).

**Key Words:** Alzheimer disease, Tau, Protein aging, Isoaspartate, Neurofibrillary tangles, Neuropil threads.

## INTRODUCTION

The abnormal intracytoplasmic inclusions referred to as neurofibrillary tangles (NFTs) and neuropil threads (NTs) are the major pathologic hallmark of tauopathies, including Alzheimer disease (AD), frontotemporal dementia, and parkinsonism linked to chromosome 17 (FTDP-17), and a number of other neurodegenerative diseases (1). Because areas forming NFTs and NTs correspond to those exhibiting neuronal loss in AD, it can be argued that the formation of these filamentous aggregates should be responsible for the neurodegeneration caused by AD and presumably by other tauopathies (2).

Various types of NFT are seen in AD brains: pretangles, intracellular (globose or flame-shaped) tangles, and extracellular (ghost) tangles (3). Pretangles may grow into globose or flame-shaped tangles (4, 5), which, in turn, are gradually converted to extracellular tangles, a tombstone of NFT-bearing neurons. The latter can be readily distinguished from intracellular tangles by their histologic and immunocytochemical staining characteristics (3, 6, 7). Because of their remarkable resistance to proteases (8–10), NFTs should be highly stable during the degeneration process and remain even after neuronal death. Thus far, only a few studies have focused on the temporal profile of NFT formation in vivo, probably as a result of the limited availability of markers for the aging of NFT.

The unit fibrils making up NFTs and NTs are called paired helical filaments (PHFs), which are 20 nm in diameter and constrict to 10 nm every 80 nm. The major component of PHFs is tau, a microtubule-associated protein that has a pivotal role in microtubule stabilization under physiological conditions (11). PHF and the tau deposited in AD brains exhibit striking characteristics: insolubility in Sarkosyl, sodium dodecyl sulfate (SDS), and urea, and smearing on SDS-PAGE (12–15). Various posttranslational modifications have been identified in tau purified from PHF-enriched fractions. Hyperphosphorylation is the best known and confers unusually slow mobility on SDS-PAGE (16–20). Ubiquitination has also been identified in the smeared tau (21). Deamidation of asparaginyl residues (Asn) and isomerization of aspartyl residues (Asp) are further modifications in the tau making up PHF smear (22).

The chemical reaction generating these can cause non-enzymatic cleavage leading to fragmentation of tau (23) and may further stabilize NFT and accelerate neurodegeneration.

Deamidation of Asn and isomerization of Asp in a protein occur spontaneously through cyclic succinimidyl intermediates, which can result in structural abnormalities and biologic dysfunction (Fig. 1) (24–27). In fact, if protein L-isoaspartyl methyltransferase, an enzyme that repairs isoAsp formation, is deleted, isomerized proteins progressively accumulate in the brain and fatal phenotypes emerge (28, 29). The tau in NFT has a rigid conformation and is not susceptible to proteases, and isoAsp-tau would accumulate with age. Thus, paired probes for Asp-tau and isoAsp-tau should provide a unique opportunity to distinguish between recent deposition and earlier deposition of tau in NFTs and NTs in the human brain (30). Thus, 2 antibodies that specifically recognize unmodified Asp-387 (numbered according to the 441-amino acid isoform of human tau) (31) and isomerized aspartyl residue (isoAsp) 387 were generated to visualize the distribution of recent and earlier deposited tau in AD brain.

## MATERIALS AND METHODS

### Subjects

Frozen brain tissues from control subjects and patients with AD were provided by Dr. A. Tamaoka (Tsukuba University Medical School) and Dr. D. J. Selkoe (Harvard Medical School). Paraffin-embedded blocks of the hippocampus from 53 subjects, including 24 patients with AD, were obtained from the Tokyo Examiner's Office (17 subjects), Tokyo Metropolitan Institute of Gerontology and Tokyo Metropolitan Geriatric Hospital (TMIG and TMG; 12 control subjects and 8 patients with AD), and Tsukuba University (16 patients with AD). The brains from TMIG and TMG were staged according to Braak and Braak (32). Vibratome sections from 15 AD brains were provided by Drs. S. Murayama and Y. Saito (Department of Neuropathology, TMIG), Dr. D. Mann (Clinical Neuroscience Research Group, University of Manchester, UK), and Dr. M. Yamazaki (Tokyo Metropolitan Institute for Neuroscience). Frozen specimens of 3 brains affected by the FTDP-17 P301L mutation (94-075, 94-079, and 96-113) and one brain affected by the R406W mutation (99-005), and paraffin-embedded sections from 3 P301L brains (97-075, 94-079, and 94-328) and one R406W brain (99-005) were from The Netherlands Brain Bank. Detailed pathologic information was provided previously (33).

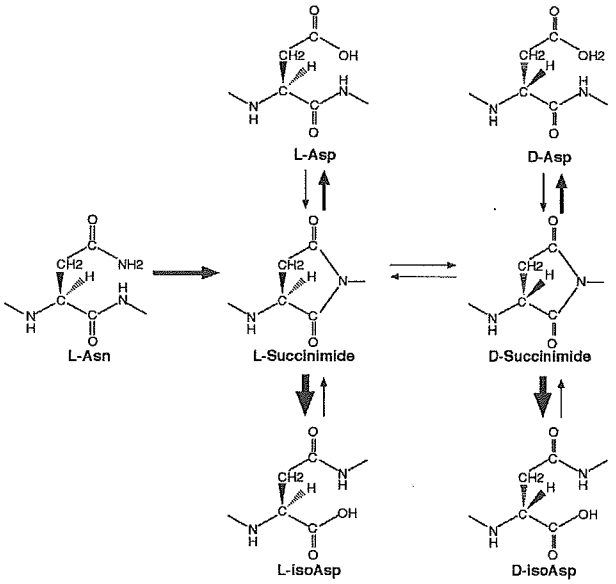


**FIGURE 1.** Schematic diagram of the isoAsp formation pathway through succinimidyl intermediate.

### Antibodies

iD387 was raised against a synthetic peptide, T(isoD) HGAEIVYK (residues 386–395) (22). The specific IgG against the isoAsp peptide was purified by 2-step affinity purification; unbound fractions eluting from a TDHGAEIVYK-immobilized column were applied to a T(iD)HGAEIVYK-immobilized column. Bound fractions were eluted and obtained as iD387. TM4, anti-Asp-387 mouse monoclonal IgG, was raised against a synthetic peptide RENAKAKTDHGAEIVYKSPVV (residues 379–399) conjugated at its carboxyl terminus with bovine serum albumin (BSA). The antigen was emulsified in complete Freund's adjuvant and injected into mouse footpads. After 2 booster injections, lymphocytes obtained from inguinal lymph nodes were fused with PAI myeloma cells. Positive clones were selected by enzyme-linked immunosorbent assay (ELISA) and Western blotting. The specificities of these 2 antibodies were assessed by ELISA. For absorption, 2.5 μg/mL of each synthetic peptide were mixed with 2.5 μg/mL TM4 or 1:250-diluted iD387 and incubated at 37°C for 30 minutes. Other mouse monoclonal antibodies used here were TM2 (pan-tau monoclonal antibody, epitope: residues 368–386) (33), HT7 (antihuman tau, residues 159–163; Innogenetics, Zwijndrecht, Belgium), AT8 (antiphosphoSer-202 and phosphoThr-205-tau; Innogenetics), and AT100 (antiphosphoThr-212 and phosphoSer-214-tau; Innogenetics).

### Tissue Fractionation and Western Blotting

Brain tissues were homogenized in Tris-saline (TS) containing a cocktail of protease inhibitors, as described previously (16). The homogenates were centrifuged at 540,000 × g for 20 minutes. The resultant TS-insoluble pellets were homogenized in 1% Sarkosyl and centrifuged again. The pellets obtained—Sarkosyl-insoluble fraction—were resuspended with 1% SDS followed by ultracentrifugation. Finally, the 1% SDS-insoluble pellets were suspended by vigorous sonication in SDS sample buffer (0.08 M Tris HCl, 2% SDS, 10% glycerol, 1% 2-mercaptoethanol, pH 6.8). Each fraction was subjected to Western blotting as described previously (33). Briefly, proteins separated on a 10% SDS-PAGE gel were electrotransferred onto a nylon membrane, which was incubated with each primary antibody. After incubation with HRP-conjugated

anti-IgG antibodies (Jackson Immunoresearch, West Grove, PA), bound antibodies were detected by enhanced chemiluminescence (ECL; Amersham, Buckingham, UK).

### Enzyme-Linked Immunosorbent Assay

ELISA plates (Nunc-Immunoplate; Nunc A/S, Roskilde, Denmark) were coated with 0.5 μg of each synthetic peptide and incubated with appropriately diluted primary antibodies. After brief washing, bound antibodies were detected with HRP-conjugated antimouse or antirabbit IgG and the color was developed by the TMB Microwell Peroxidase Substrate system (Kirkegaard and Perry Laboratories, Gaithersburg, MD).

### Immunocytochemistry

Paraffin-embedded sections were immunostained as described previously (33). To determine the optimal staining conditions for these antibodies, various pretreatments were tested, including pretreatment with 0.5% Triton X-100, target retrieval solution (DakoCytomation, Carpinteria, CA), 95% formic acid, by autoclaving, and pretreatment by autoclaving followed with formic acid. We found that treatment with 95% formic acid for 4 minutes provides the optimum for AT8 staining, and treatment by autoclaving at 120°C for 7 minutes followed with 95% formic acid for 4 minutes for TM2-, TM4-, and iD387-staining (34). After pretreatment, sections were incubated with primary antibodies overnight at room temperature, incubated with biotinylated antimouse or antirabbit IgG (Vector Laboratories, Inc., Burlingame, CA), and finally with avidin and biotinylated HRP (Vectastain ABC kit; Vector Laboratories, Inc.). Bound antibodies were visualized with 3,3′-diaminobenzidine (DAB) in the presence of hydrogen peroxide, and the DAB-developed sections were briefly counterstained with hematoxylin. Semiquantification of NFT was performed as described previously (34). TM2- or TM4-positive NFTs were counted, and their numbers were averaged across 3 nonselected areas of 3.2 $mm^2$.

For confocal microscopy, 30- to 50-μm thick vibratome sections from AD cerebral cortex were pretreated with 95% formic acid followed by incubation with primary antibodies. This treatment provided better conditions for the staining of tau inclusions with TM4 and iD387, compared with no treatment or 0.5% Triton X-100 treatment (data not shown). Bound antibodies were visualized with Alexa 488-conjugated antimouse IgG or Alexa 568-conjugated antirabbit IgG (Molecular Probes, Inc., Eugene, OR). When necessary, lipofuscin autofluorescence was eliminated with Sudan Black B, as described previously (35). Specimens were observed under a Zeiss Axioskop microscope (Carl Zeiss Inc., Thornwood, NY) equipped with the Lasersharp2000 software (Bio-Rad Laboratories).

## RESULTS

### Characterization of Asp-387-Specific, and isoAsp-387-Specific Antibodies

Three major deamidation/isomerization sites, Asp-193, Asn-381, and Asp-387, were previously identified in the PHF-smear (22) (Fig. 1). iD387 was raised against a synthetic peptide containing isoAsp-387 (Fig. 2A). On the ELISA plate, iD387 preferentially reacted with the isoAsp peptide, but scarcely with the unmodified Asp peptide (Fig. 2B). However, this antibody crossreacted to some extent with dextro-isoAsp-387 (diD387) peptide, a minor product in the isoAsp formation reaction (36) (Fig. 1). The Asn-381-modified peptide had no effect on the reactivities of these antibodies (data not shown). In contrast, TM4, raised against residues 379–399 (Fig. 2A), reacted exclusively with unmodified Asp-387 peptide and not with isoAsp-387 peptide (Fig. 2B). The effect of preabsorption was also assessed by Western blotting (Fig. 2C). TM4 labeling of recombinant tau was greatly reduced by preabsorption with L-Asp peptide but not with L-isoAsp peptide. Thus, TM4 specifically labels unmodified Asp-387-containing tau. Furthermore, the specificity of these 2 antibodies was examined by immunocytochemistry. Combined treatment by autoclaving and formic acid was found to be the most effective for immunostaining with TM2, TM4, and iD387 (data not shown). Under this condition, TM4 intensely labeled NFTs in AD brains, staining being abolished by preabsorption with Asp-peptide (Fig. 2D). Despite strong labeling of normal (soluble) tau on Western blots, TM4 does not obviously stain unaffected neurons in which abundant normal tau should exist. This may reflect the characteristics of tau: unmodified tau is normally unfolded and susceptible to formalin fixation, whereas modified (especially phosphorylated) tau has a particular conformation, which is resistant to fixation (37). On the other hand, preabsorption with L-isoAsp peptide completely eliminated the immunoreactivity of iD387 for NFTs (Fig. 2D).

### Western blotting of Insoluble Fractions Using Asp-387- and isoAsp-387-Specific Antibodies

To assess the extent of isoAsp-387 formation, Sarkosyl-insoluble and SDS-insoluble fractions from control and AD brains were subjected to Western blotting using TM4, iD387, and other tau antibodies. The Sarkosyl-insoluble tau in AD brains is characterized by the presence of PHF-tau and PHF smear on the blots (21).

TM2, the epitope of which is located in residues 368–386 (Fig. 2A), intensely labeled PHF smear in the Sarkosyl-insoluble and SDS-insoluble fractions from AD brain (Fig. 3A). HT7, AT8, and AT100, the epitopes of which are located in the aminoterminal half or midportion of tau (see "Materials and Methods" for detailed information), strongly labeled 3 (or 4) bands of PHF-tau, but only faintly labeled PHF smear, especially the smear in the SDS-insoluble fraction (Fig. 3B–D). This indicates that the aminoterminal portion is lost in PHF smear and that AT8 can detect only a fraction of detergent-insoluble tau. This is consistent with previous reports on the selective concentration of the carboxyl-third of tau in PHF smear (21, 22).

As noted, PHF-tau was recovered exclusively in the Sarkosyl-insoluble, SDS-soluble fraction, whereas PHF smear was left in the SDS-insoluble fraction. The SDS-insoluble smear stayed in the stacking gel, whereas the SDS-soluble smear entered the separating gel and extended from high-molecular-weight to low-molecular-weight regions (Fig. 3A). These data suggest that filaments made of PHF smear are more resistant to SDS than those of PHF-tau. Such insoluble tau was

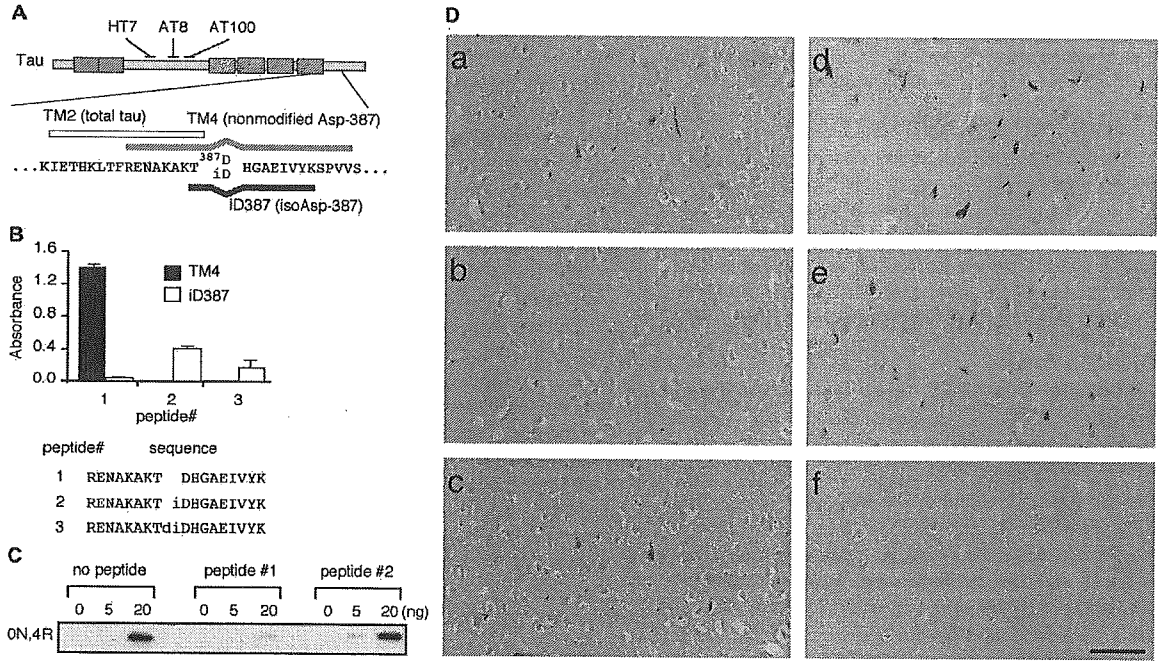


FIGURE 2. Characterization of TM4 and iD387. **(A)** The antibodies used in this study and the locations of their epitopes along the longest, 441-residue human tau molecule (dark gray boxes, aminoterminal inserts; striped boxes, microtubule-binding domains). The gray and black bars indicate the immunogens for TM4 and iD387, respectively. ID, isoAsp-387. **(B)** Specificities of TM4 and iD387 toward isomerized and unmodified synthetic peptides as assessed by one-site enzyme-linked immunosorbent assay. A plate coated with 2.5 μg of either peptide (residues 379–395 of tau; lower panel) was incubated with either TM4 or iD387. TM4 reacted only with unmodified peptide (peptide 1). iD387 strongly labeled isoAsp-peptide (2), but scarcely Asp-peptide (1). Dextro-isoAsp (diD) peptide (3) was partially labeled with iD387, but not with TM4. Bars indicate means ± standard error of 3 independent experiments. **(C)** Indicated amounts of recombinant 0N4R tau were subjected to Western blotting using TM4 or TM4 preabsorbed with Asp- or isoAsp-peptide. The TM4 immunoreactivity is markedly reduced by preabsorption with Asp-peptide (1) but not with isoAsp-peptide (2). **(D)** To test the specificity at the immunocytochemical level, AD sections were probed with TM4 **(a–c)** and iD387 **(d–f)** preabsorbed without **(a, d)** or with Asp-peptide (1, **[b, e]**) and isoAsp-peptide (2, **[c, f]**). TM4 or iD387 staining was completely abolished by preabsorption with Asp-peptide (1, **[b]**) or isoAsp-peptide (2, **[f]**), respectively. Scale bar = 50 μm.

never found in the corresponding fractions from control brains (Fig. 3A).

TS-soluble tau in control and AD brains was labeled with TM4 but never with iD387 (data not shown). TM4 preferentially labeled PHF-tau in the Sarkosyl-insoluble, SDS-soluble fraction, but only faintly labeled PHF smear (Fig. 3E). In contrast, iD387 intensely labeled PHF smear in SDS-soluble and SDS-insoluble fractions (Fig. 3F). This is consistent with the view that PHF become progressively insoluble and that PHF-tau is gradually converted to PHF smear in vivo (21). Thus, it is reasonable to postulate that TM4-labeled tau represents the more recent tau deposition and iD387-labeled tau represents an earlier deposition.

## Tau Inclusions Labeled With Asp-387- and isoAsp-387-Specific Antibodies

NFTs, NTs, and dystrophic neurites (DNs; senile plaque-associated neurites) were examined for the extent of TM4 and iD387 immunoreactivities compared with TM2 immunoreactivity. TM2 was assumed to label all intra- and extracellular NFTs, because its epitope is located in the "PHF core" (Fig. 4A, E) (10). In contrast, AT8 failed to label extracellular NFTs, because the epitope is lost in those tangles, possibly as a result of proteolytic processing (Fig. 3).

We have focused on the hippocampus, the most vulnerable area in AD, which contains all types of NFTs—pre-tangles, intracellular, and extracellular, tangles—in varying proportions (5, 38). In Braak stages III/IV, TM2 intensely labeled NFTs and NTs in the CA1 region. The densely packed flame-shaped NFTs surrounding the nucleus are representative of intracellular NFTs. In adjacent sections, these NFTs were labeled with both TM4 and iD387 (Fig. 4A–D). NTs were well labeled, but more intensely with iD387. DNs were labeled to the same extent with both antibodies. In the hippocampus at Braak stages V/VI, TM2 labeled innumerable NFTs (Fig. 4E). These were mostly extracellular NFTs, because of their flattened configuration and the absence of nuclei. These NFTs, except for a few, were hardly labeled with TM4 (Fig. 4F). This suggests that extracellular NFTs are mainly composed of tau containing modified Asp-387. However, unexpectedly, only a small fraction of the extracellular NFTs was labeled strongly with iD387, whereas the remainder was only faintly stained (Fig. 4G). NTs in the brains at Braak stages V/VI were also scarcely labeled with TM4 or iD387 (data not shown).

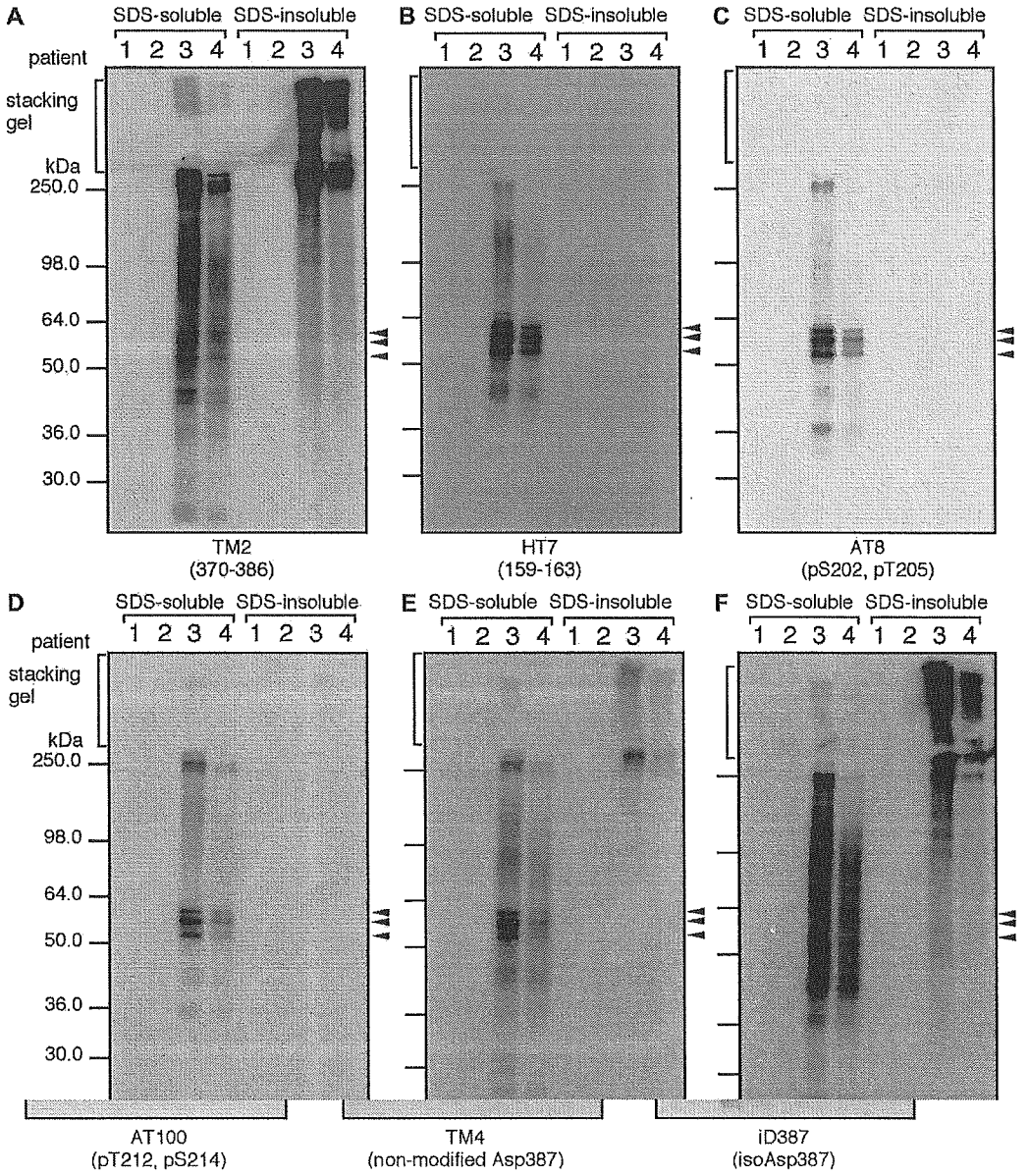


**FIGURE 3.** Full-length PHF-tau and PHF smear as labeled with TM4 or iD387. Sarkosyl-insoluble pellets from control (lanes 1 and 2) and AD (lanes 3 and 4) brains were further fractionated by solubility in 1% SDS. Each fractionated sample was subjected to Western blotting using the indicated antibodies. TM2, a pan-tau antibody, labeled characteristic triplet bands composing PHF-tau (arrowheads) and PHF smear **(A)**. In sharp contrast, HT7 **(B)**, AT8 **(C)**, and AT100 **(D)**, intensely labeled PHF-tau but not PHF smear, indicating loss of the aminoterminal and midportions in PHF smear. The same fractions were also subjected to Western blotting with TM4 **(E)** and iD387 **(F)**. Although the epitopes of TM4 and TM2 are located very closely (see Fig. 2), TM4 intensely labeled PHF-tau, but only weakly PHF smear in the SDS-soluble fraction and barely PHF smear in the SDS-insoluble fraction. In contrast, iD387 intensely labeled PHF smear in both SDS-soluble and insoluble fractions, which overshadowed PHF-tau.

TM2-positive and TM4-positive NFTs were quantified in the CA1 region. Because the isomerization of Asp is a spontaneous chemical reaction, the rate of isoAsp formation in PHFs can be regarded as not so variable. Thus, TM4-positive NFT counts reflect the generation rate of NFT-bearing neurons at the time of death. Along with the total numbers of NFT, mild (0–50/3.2 $mm^2$), moderate (51–100/3.2 $mm^2$), advanced (101–150/3.2 $mm^2$), and severe (over 151/3.2 $mm^2$), those of TM4-positive NFT increased from mild to moderate cases, but rather leveled off in moderate to severe cases (Fig. 5). Statistically

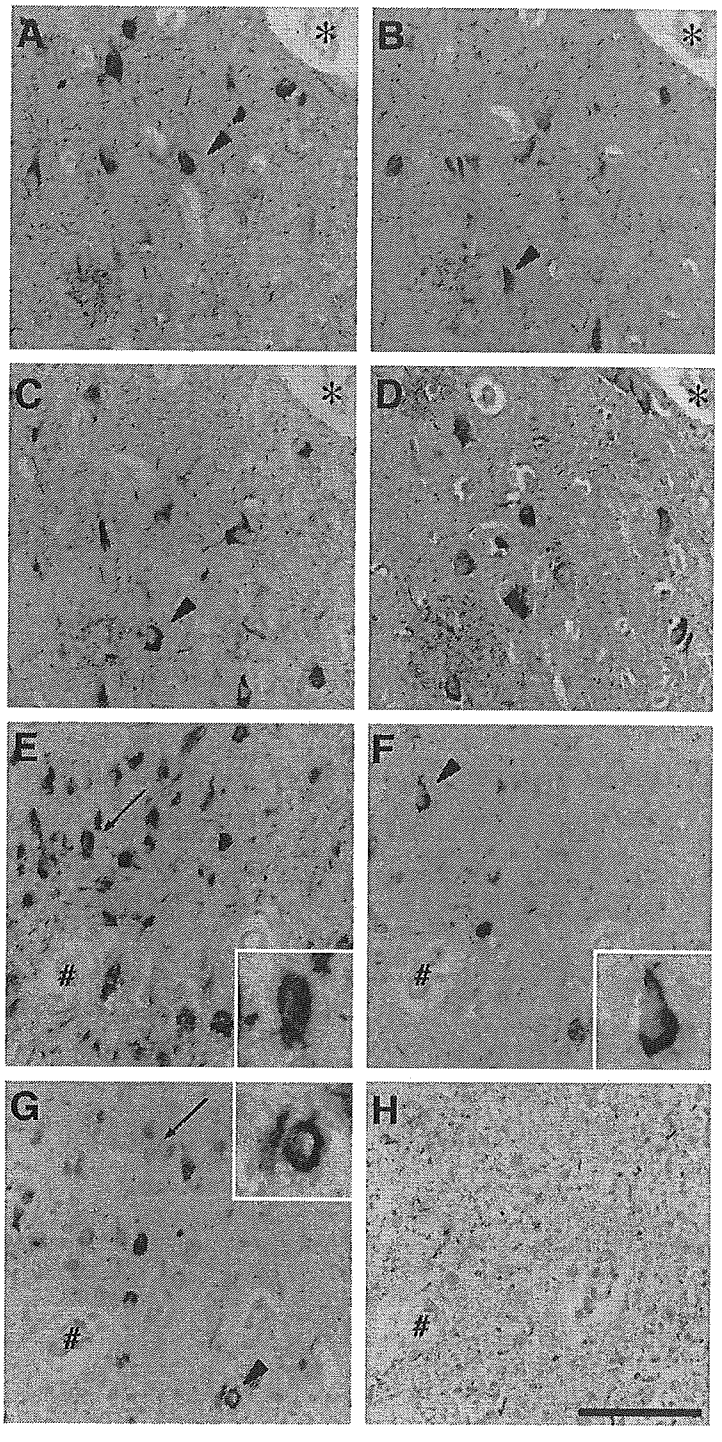


FIGURE 4. Immunocytochemistry using TM4 and iD387. Paraffin-embedded sections from the hippocampus at Braak stages III/IV (**A–D**) and Braak stage V/VI (**E–H**) were immunostained with TM2 (**A, E**), TM4 (**B, F**), iD387 (**C, G**), and AT8 (**D, H**). Note that all antibodies intensely stained intracellular neurofibrillary tangles (NFTs) (arrowheads and inset) and neuropil threads in the hippocampus at the early neocortical stage (**A–D**). In contrast, extracellular NFTs (arrows and inset) were hardly stained with TM4 (**F**) or iD387 (**G**) and were not stained with AT8 (**H**). *, # indicate the same vessels in adjacent sections. Scale bar = 100 μm.

significant differences in the TM4-positive NFT counts were observed only between mild and moderate cases (Fig. 5). Thus, TM4-positive NFT appeared to be constant even though the total NFT number increased from moderate to severe cases. This unexpected finding raises the possibility that NFTs are produced at a constant rate irrespective of the disease stage and are also constantly converted to TM4-negative (extracellular) NFTs in the hippocampus.

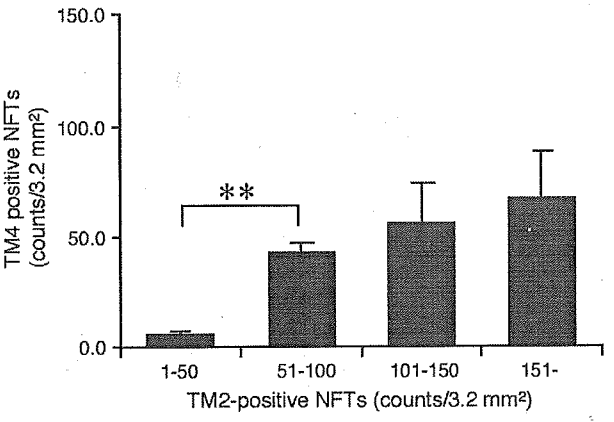


FIGURE 5. Semiquantification of TM2- and TM4-positive neurofibrillary tangles (NFTs) in the hippocampus. TM2- and TM4-positive NFTs per 3.2 mm² in the hippocampi of 53 non-Alzheimer disease (control) subjects and patients with Alzheimer disease were counted. The numbers of TM4-positive NFTs are shown against the abundance of TM2-positive NFTs: mild (0–50, n = 23), moderate (51–100, n = 14), advanced (101–150, n = 6), and severe (>151, n = 9). The numbers of TM4-positive NFTs significantly increased from mild to moderate cases, but not so from moderate to severe cases. Means ± standard error. Statistically evaluated by 2-way analysis of variance, followed by Bonferroni/Dunn post hoc test. Asterisks indicate a statistically significant difference (**, $p < 0.01$).

## Distinct Localization of Isomerized and Unmodified tau

To investigate the localization of Asp-387 and isoAsp-387 in NFTs and NTs, vibratome sections from the hippocampus or temporal cortex at Braak stage IV or above were double-stained with TM4 and iD387 and viewed under a confocal laser-scanning microscope. The specimens from 8 of 15 subjects were labeled with both antibodies, the remainder being labeled only with iD387. Storage of the specimens seemed to have a remarkable effect on the extent of TM4 and iD387 staining. Vibratome sections stored in sucrose at –20°C were not stainable with TM4, whereas iD387 staining was retained. This was not the case with paraffin-embedded sections or immediately frozen blocks. It is likely therefore that isoAsp formation through succinimidyl intermediates proceeds in the aqueous environment, irrespective of prior formalin fixation.

In the specimens from the 8 subjects, NFTs were labeled with both antibodies, whereas NTs were labeled predominantly with iD387. In 6 cases, NTs were labeled to a similar extent with these 2 antibodies. Double immunostaining clearly showed that the portions labeled with the 2 antibodies were distinct from each other. TM4 stained NFTs in proximal dendrites and neuronal perikarya, whereas iD387 stained NFTs up to more distal dendrites (Fig. 6A, B). The intensities of TM4 and iD387 staining varied even within a thread (Fig. 6C). Most commonly, TM4 intensely labeled the outer portion of a thread, and iD387 preferentially labeled its core portion (Fig. 6D, E). In the case of isoAsp-387-rich NTs, patchy and discrete TM4 staining on the surface of a thread was often evident (Fig. 6D). In general, DNs were better stained with TM4, and NTs were better stained with iD387 (Fig. 6F).

## Isomerization of tau in P301L and R406W Brains

More than 30 exonic and intronic mutations have been identified in the tau gene in patients affected by frontotemporal dementia and parkinsonism linked to chromosome 17 (FTDP-17), which is characterized pathologically by extensive neuronal loss and formation of filaments composed of tau (39, 40). Among FTDP-17 mutations, the P301L mutation is well known for its aggressive clinical phenotype and the R406W mutation for its more slowly progressive phenotype (41). It is possible that some differences between P301L and R406W mutations, including the type of tau deposited (4R tau vs. 3R + 4R tau), distribution of the tau pathology (widespread vs. rather restricted), and the differences in the cell type affected (neuronal and glial cells vs. neuronal cells), may be related to the difference in the phenotype. To determine whether isomerization of the deposited tau occurs similarly in these brains, Sarkosyl-insoluble fractions from affected frontal cortices were prepared and subjected to Western blotting using TM2, TM4, and iD387. TM2 intensely labeled the PHF smear in the Sarkosyl-insoluble fraction from a R406W brain. In contrast, only 2 major bands at 64 and 68 kDa were labeled in P301L brains (Fig. 7). These results are consistent with previous reports (23, 33, 34). TM4 labeled 3 bands of PHF-tau in AD and R406W brains, and 2 major bands in P301L brains, but only faintly PHF smear. In contrast, iD387 labeled exclusively PHF smear in AD and R406W brains but none in P301L brains (Fig. 7). Thus, the Sarkosyl-insoluble tau from R406W brains is isomerized at Asp-387 to a much greater extent than in P301L brains. Immunocytochemical staining of P301L and R406W brains with these antibodies was also examined. In a P301L case, TM2 and TM4 stained innumerable pretangles in the frontal cortex, but iD387 did only faintly (data not shown). In contrast, NFTs in R406W brain were intensely stained with both antibodies. This is consistent with the Western blot data shown in Figure 7.

## DISCUSSION

Differential visualization of Asp- (unmodified) and isoAsp- (modified) tau should provide us with a time window for the formation and evolution of tau inclusions in the human brain. As shown here, there is a much larger amount of isoAsp-387 in PHF smear than in PHF-tau. Thus, TM4 and iD387 make it possible to visualize recent and earlier deposited tau proteins, respectively. Although the rate of isoAsp formation in PHFs in vivo is unknown, an in vitro incubation study showed that isoAsp-387 tau is gradually generated and discrete tau bands are converted to a smear over months (23). Thus, it is reasonable to assume that the formation of PHF smear takes months, but not longer than years.

TM4 intensely immunostained intracellular NFTs, but hardly stained the most evolved extracellular NFTs. According

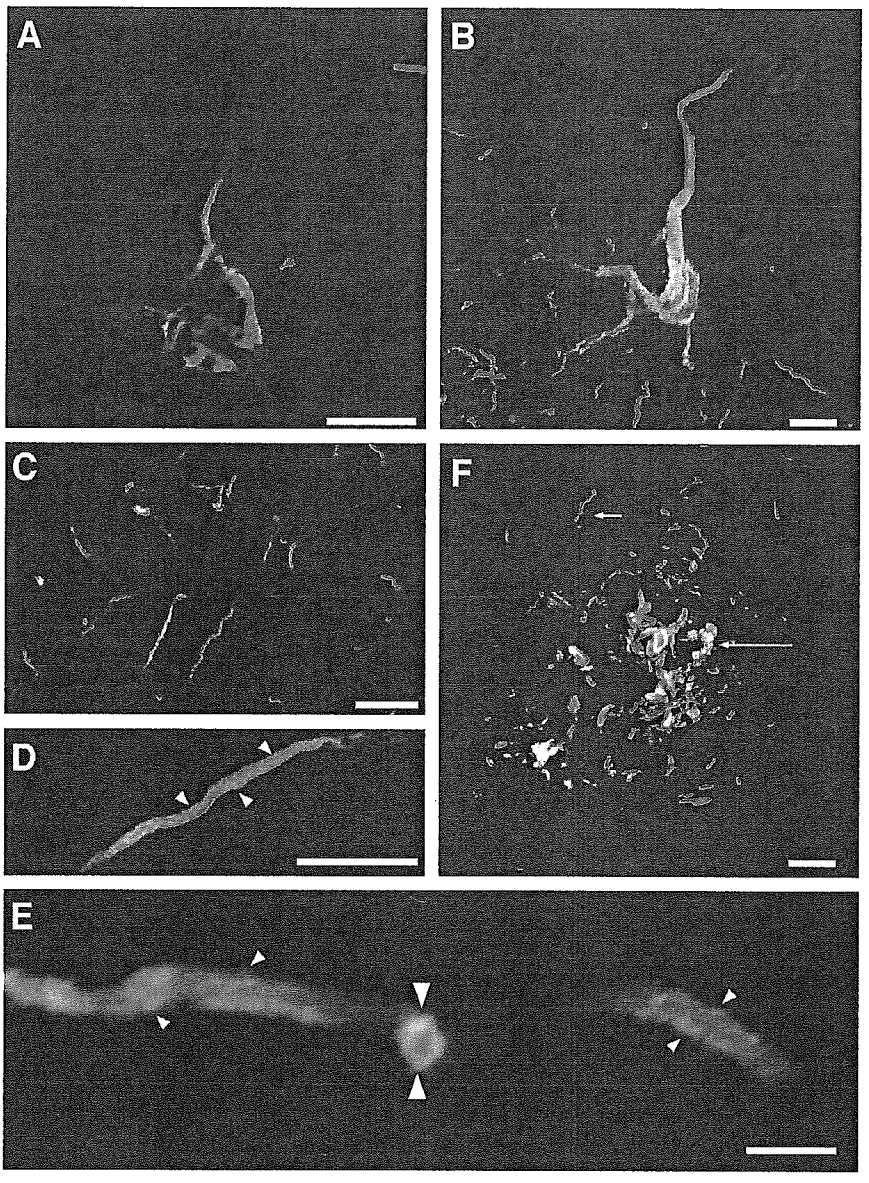


**FIGURE 6.** Differential distribution of TM4- and iD387-positive tau in neurofibrillary tangle (NFT), neuropil thread (NT), and dystrophic neurite (DN). Vibratome sections from Alzheimer disease temporal cortices or hippocampi were labeled with TM4 (green) and iD387 (red), and observed under a confocal microscope. Merged images in the temporal cortices of patient 1 **(A, F)** and patient 2 **(B)**, and in the hippocampus of patient 3 **(C)** are shown. TM4 preferentially labeled the NFTs in the proximal portion of dendrites and cell bodies, whereas iD387 labeled whole profiles of NFTs up to the distal potion of dendrites **(A, B)**. TM4 and iD387 immunoreactivities of NTs varied substantially **(C)**. When TM4 immunoreactivity is noticeable on NT, it is mostly located on its outer portion **([D, E]**, small arrowheads). A transverse section clearly shows that TM4 labeled the outer portion of a thread **([E]**, large arrowhead), whereas iD387 labeled the core portion. TM4 stained DNs (long arrow) to a greater extent than scattered NTs in the surrounding area (short arrow) **(F)**. Scale bars = **(A–D, F)** 10 μm; **(E)** 2 μm.

to recent studies, NFT-bearing neurons can live decades (42) and the maturation of NFT takes several years (43). Together with our results shown in Figure 4, the presence of unmodified tau, even in the terminal stages of NFTs, suggests that de novo synthesis of tau (and possibly other proteins) is still maintained in such degenerating neurons. Infrequently encountered TM4-labeled, apparently extracellular NFTs based on their morphology support this assumption (data not shown).

We do not know why iD387 stained only faintly the majority of extracellular NFTs. It is possible that carboxyl-terminal processing of tau could have eliminated isoAsp-387. Nonenzymatic cleavage of tau at this site proceeds for months, as shown by prolonged in vitro incubation of recombinant tau (23). This possibility may be supported by the weak labeling of extracellular NFTs with PHF-1, the epitope of which (phosphoSer-396 and phosphoSer-404) is ~10 residues downstream of Asp-387 (data not shown). Another possibility is that Asp-387 in NFT undergoes further modifications such as racemization (Fig. 1) (36). Related to this, the decreased reactivity of iD387 with dextro-isoAsp-387 is of particular interest (Fig. 2B).

In this study, we hypothesized that TM4-positive NFT counts reflect the generation rate of NFT-bearing neurons. Based on these indices, it is likely that the generation rate is lowest in mild cases, presumably at Braak stages I/II (32). Subsequently, a rather constant generation rate may follow in

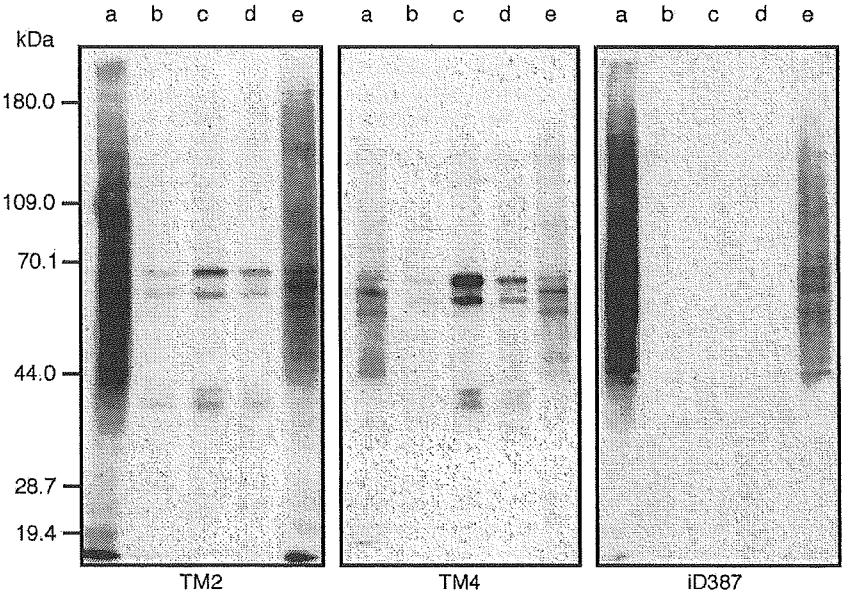


FIGURE 7. IsoAsp formation in the Sarkosyl-insoluble tau in P301L and R406W brains. Sarkosyl-insoluble fractions were prepared from the frontal cortices of one patient with Alzheimer disease (AD) **(a)**, 3 P301L patients **([b]**: 94-075, **[c]**: 94-079, and **[d]**: 96-113), and one R406W patient **([e]**: 99-005), and were subjected to Western blotting using TM2, TM4, and iD387. TM2 detected the PHF smear in AD and R406W cortices, and labeled 2 major bands at 64 and 68 kDa in P301L specimens. iD387 strongly labeled the insoluble smeared tau from an R406W brain, but none from P301L brains. In contrast, TM4 strongly labeled discrete triplet bands in the specimens from AD and R406W brains and 2 bands in the specimens from P301L brains.

moderate to severe cases, which may correspond to Braak stages III to VI. This leads us to postulate the following chronology of NFT formation. In the early phase, tau is slowly deposited in the cytoplasm of large (mostly pyramidal) neuron, likely as pretangles. Presumably, this is the critical period for NFT formation. In Braak stages III/IV, when senile plaques appear in the CA1 region, NFTs are constantly generated and new NFT formation continues until Braak stages V/VI. Finally, NFT-bearing neurons die, and new tau deposition is no longer seen in CA1 neurons at Braak stages V/VI. This assumption can be tested if the 2 antibodies used here were applied to a mouse model showing both amyloid plaques and NFTs (44).

The most striking finding is the differential distribution of Asp-387 and isoAsp-387 in NFTs and NTs in the hippocampus and temporal cortex. Whereas iD387 intensely labeled whole profiles of NFTs up to distal branches of the dendrite, TM4 preferentially stained NFTs in the proximal dendritic portion and perikaryon. This may reflect continued protein biosynthesis in the proximal dendrites and perikarya, and dysfunction of the trafficking required for normal intracellular transport of tau or tau mRNA (45). In the affected neurons, newly synthesized tau or tau mRNA cannot be transported to the distal dendrites and accumulates in the proximal dendrites and cell body, which may further displace intracellular organelles and affect cellular metabolism. This view is supported by repeated observations that tubulin immunoreactivity is completely abolished or displaced to the periphery in NFT-bearing neuronal perikarya (46).

The outer portion of a thread was intensely stained with TM4. Together with the predominant staining of the core portion with iD387, this strongly suggests that NTs constantly gain diameter by addition of newly produced tau (or PHF) on their surface. When NT-containing neurites (mostly dendrites) are disconnected from the cell body, new tau deposition onto NTs ceases and the tau on the outer surface may become gradually deamidated and isomerized. NTs that are exclusively stained with iD387 may represent such a kind of extracellular NTs.

Western blots of specimens from R406W brains showed the presence of isoAsp-387 in the insoluble tau to similar extents as observed in AD brains. This indicates that the NFTs in the R406W brains progressively evolve, and isoAsp-387 increasingly accumulates like in AD brains. In contrast, in P301L brains, none was labeled with iD387. The insoluble tau in P301L brains would be deposited for too short a period for Asp to be converted to isoAsp and cleared rapidly by neuronal death. These may explain the disparity in the clinical and pathologic features of these 2 mutations: P301L is representative of a rapidly progressive phenotype (early onset and short duration), whereas R406W is of a more slowly progressive and mild phenotype (41). Another possible explanation is that the deposited tau, largely mutant P301L tau (34), is structurally weak and swiftly removed by enhanced cellular degradation systems before isoAsp formation, and affected neurons maintain the levels of modified tau very low.

## ACKNOWLEDGMENTS

*The authors thank Drs. A. Tamaoka and D. J. Selkoe, and M. Yoshimura for providing some of the cases used in this study, and Ms. J. Saishoji and N. Naoi for their technical assistance.*

## REFERENCES

1. Lee VM, Goedert M, Trojanowski JQ. Neurodegenerative tauopathies. Annu Rev Neurosci 2001;24:1121–59
2. Gomez-Isla T, Hollister R, West H, et al. Neuronal loss correlates with but exceeds neurofibrillary tangles in Alzheimer's disease. Ann Neurol 1997; 41:17–24

3. Braak E, Braak H, Mandelkow EM. A sequence of cytoskeleton changes related to the formation of neurofibrillary tangles and neuropil threads. Acta Neuropathol (Berl) 1994;87:554–67
4. Uchihara T, Nakamura A, Yamazaki M, Mori O. Evolution from pretangle neurons to neurofibrillary tangles monitored by thiazin red combined with Gallyas method and double immunofluorescence. Acta Neuropathol (Berl) 2001;101:535–39
5. Uboga NV, Price JL. Formation of diffuse and fibrillar tangles in aging and early Alzheimer's disease. Neurobiol Aging 2000;21:1–10
6. Brion JP, Hanger DP, Bruce MT, Couck AM, Flament-Durand J, Anderton BH. Tau in Alzheimer neurofibrillary tangles. N- and C-terminal regions are differentially associated with paired helical filaments and the location of a putative abnormal phosphorylation site. Biochem J 1991; 273:127–33
7. Uchihara T, Nakamura A, Yamazaki M, Mori O, Ikeda K, Tsuchiya K. Different conformation of neuronal tau deposits distinguished by double immunofluorescence with AT8 and thiazin red combined with Gallyas method. Acta Neuropathol (Berl) 2001;102:462–66
8. Yen SH, Kress Y. The effect of chemical reagents or proteases on the ultrastructure of paired helical filaments. In: Katzman R, ed. *Biological Aspects of Alzheimer's Disease (Banbury report 15)*. New York: Cold Spring Harbor Laboratory, 1983
9. Selkoe DJ, Ihara Y, Abraham C, Rasool CG, McCluskey AH. Biochemical and immunochemical studies of Alzheimer paired helical filaments. In: Katzman R, ed. *Biological Aspects of Alzheimer's Disease (Banbury Report 15)*. New York: Cold Spring Harbor Laboratory, 1985:125–34
10. Wischik CM, Novak M, Thogersen HC, et al. Isolation of a fragment of tau derived from the core of the paired helical filament of Alzheimer disease. Proc Natl Acad Sci USA 1988;85:4506–10
11. Lee VM. Disruption of the cytoskeleton in Alzheimer's disease. Curr Opin Neurobiol 1995;5:663–68
12. Selkoe DJ, Ihara Y, Salazar FJ. Alzheimer's disease: Insolubility of partially purified paired helical filaments in sodium dodecyl sulfate and urea. Science 1982;215:1243–45
13. Ihara Y, Abraham C, Selkoe DJ. Antibodies to paired helical filaments in Alzheimer's disease do not recognize normal brain proteins. Nature 1983;304:727–30
14. Greenberg SG, Davies P. A preparation of Alzheimer paired helical filaments that displays distinct tau proteins by polyacrylamide gel electrophoresis. Proc Natl Acad Sci USA 1990;87:5827–31
15. Lee VM, Balin BJ, Otvos L Jr., Trojanowski JQ. A68: A major subunit of paired helical filaments and derivatized forms of normal Tau. Science 1991;251:675–78
16. Hasegawa M, Morishima-Kawashima M, Takio K, Suzuki M, Titani K, Ihara Y. Protein sequence and mass spectrometric analyses of tau in the Alzheimer's disease brain. J Biol Chem 1992;267:17047–54
17. Hasegawa M, Watanabe A, Takio K, et al. Characterization of two distinct monoclonal antibodies to paired helical filaments: Further evidence for fetal-type phosphorylation of the tau in paired helical filaments. J Neurochem 1993;60:2068–77
18. Morishima-Kawashima M, Hasegawa M, Takio K, et al. Proline-directed and non-proline-directed phosphorylation of PHF-tau. J Biol Chem 1995; 270:823–29
19. Morishima-Kawashima M, Hasegawa M, Takio K, et al. Hyperphosphorylation of tau in PHF. Neurobiol Aging 1995;16:365-71; discussion 71–80
20. Goedert M, Spillantini MG, Cairns NJ, Crowther RA. Tau proteins of Alzheimer paired helical filaments: Abnormal phosphorylation of all six brain isoforms. Neuron 1992;8:159–68
21. Morishima-Kawashima M, Hasegawa M, Takio K, Suzuki M, Titani K, Ihara Y. Ubiquitin is conjugated with amino-terminally processed tau in paired helical filaments. Neuron 1993;10:1151–60
22. Watanabe A, Takio K, Ihara Y. Deamidation and isoaspartate formation in smeared tau in paired helical filaments. Unusual properties of the microtubule-binding domain of tau. J Biol Chem 1999;274:7368–78
23. Watanabe A, Hong WK, Dohmae N, Takio K, Morishima-Kawashima M, Ihara Y. Molecular aging of tau: Disulfide-independent aggregation and non-enzymatic degradation in vitro and in vivo. J Neurochem 2004;90:1302–11
24. Chazin WJ, Kordel J, Thulin E, Hofmann T, Drakenberg T, Forsen S. Identification of an isoaspartyl linkage formed upon deamidation of bovine calbindin D9k and structural characterization by 2D 1H NMR. Biochemistry 1989;28:8646–53
25. Brennan TV, Anderson JW, Jia Z, Waygood EB Clarke S. Repair of spontaneously deamidated HPr phosphocarrier protein catalyzed by the L-isoaspartate-(D-aspartate) O-methyltransferase. J Biol Chem 1994;269: 24586–95
26. George-Nascimento C, Lowenson J, Borissenko M, et al. Replacement of a labile aspartyl residue increases the stability of human epidermal growth factor. Biochemistry 1990;29:9584–91
27. Johnson BA, Langmack EL, Aswad DW. Partial repair of deamidation-damaged calmodulin by protein carboxyl methyltransferase. J Biol Chem 1987;262:12283–87
28. Kim E, Lowenson JD, MacLaren DC, Clarke S, Young SG. Deficiency of a protein-repair enzyme results in the accumulation of altered proteins, retardation of growth, and fatal seizures in mice. Proc Natl Acad Sci USA 1997;94:6132–37
29. Yamamoto A, Takagi H, Kitamura D, et al. Deficiency in protein L-isoaspartyl methyltransferase results in a fatal progressive epilepsy. J Neurosci 1998;18:2063–74
30. Fonseca MI, Head E, Velazquez P, Cotman CW, Tenner AJ. The presence of isoaspartic acid in beta-amyloid plaques indicates plaque age. Exp Neurol 1999;157:277–88
31. Goedert M, Spillantini MG, Jakes R, Rutherford D, Crowther RA. Multiple isoforms of human microtubule-associated protein tau: Sequences and localization in neurofibrillary tangles of Alzheimer's disease. Neuron 1989;3:519–26
32. Braak H, Braak E. Neuropathological staging of Alzheimer-related changes. Acta Neuropathol (Berl) 1991;82:239–59
33. Miyasaka T, Morishima-Kawashima M, Ravid R, et al. Molecular analysis of mutant and wild-type tau deposited in the brain affected by the FTDP-17 R406W mutation. Am J Pathol 2001;158:373–79
34. Miyasaka T, Morishima-Kawashima M, Ravid R, Kamphorst W, Nagashima K, Ihara Y. Selective deposition of mutant tau in the FTDP-17 brain affected by the P301L mutation. J Neuropathol Exp Neurol 2001; 60:872–84
35. Schnell SA, Staines WA, Wessendorf MW. Reduction of lipofuscin-like autofluorescence in fluorescently labeled tissue. J Histochem Cytochem 1999;47:719–30
36. Lowenson JD, Clarke S. Recognition of D-aspartyl residues in polypeptides by the erythrocyte L-isoaspartyl/D-aspartyl protein methyltransferase. Implications for the repair hypothesis. J Biol Chem 1992;267: 5985–95
37. Trojanowski JQ, Schuck T, Schmidt ML, Lee VM. Distribution of tau proteins in the normal human central and peripheral nervous system. J Histochem Cytochem 1989;37:209–15
38. Augustinack JC, Schneider A, Mandelkow EM, Hyman BT. Specific tau phosphorylation sites correlate with severity of neuronal cytopathology in Alzheimer's disease. Acta Neuropathol (Berl) 2002;103:26–35
39. Brandt R, Hundelt M, Shahani N. Tau alteration and neuronal degeneration in tauopathies: Mechanisms and models. Biochim Biophys Acta 2005;1739:331–54
40. Goedert M, Jakes R. Mutations causing neurodegenerative tauopathies. Biochim Biophys Acta 2005;1739:240–50
41. van Swieten JC, Stevens M, Rosso SM, et al. Phenotypic variation in hereditary frontotemporal dementia with tau mutations. Ann Neurol 1999;46:617–26
42. Morsch R, Simon W, Coleman PD. Neurons may live for decades with neurofibrillary tangles. J Neuropathol Exp Neurol 1999;58:188–97
43. Bobinski M, Wegiel J, Tarnawski M, et al. Duration of neurofibrillary changes in the hippocampal pyramidal neurons. Brain Res 1998;799:156–58
44. Lewis J, Dickson DW, Lin WL, et al. Enhanced neurofibrillary degeneration in transgenic mice expressing mutant tau and APP. Science 2001;293: 1487–91
45. Litman P, Barg J, Ginzburg I. Microtubules are involved in the localization of tau mRNA in primary neuronal cell cultures. Neuron 1994;13: 1463–74
46. Hempen B, Brion JP. Reduction of acetylated alpha-tubulin immunoreactivity in neurofibrillary tangle-bearing neurons in Alzheimer's disease. J Neuropathol Exp Neurol 1996;55:964–72

Available online at www.sciencedirect.com
SCIENCE DIRECT®
Analytical Biochemistry 347 (2005) 106–111
ANALYTICAL BIOCHEMISTRY
www.elsevier.com/locate/yabio

# More than a 100-fold increase in immunoblot signals of laser-microdissected inclusion bodies with an excessive aggregation property by oligomeric actin interacting protein 2/D-lactate dehydrogenase protein 2

Naomi S. Hachiya [a], Takuya Ohkubo [b], Yoshimichi Kozuka [c], Mineo Yamazaki [d], Osamu Mori [e], Hidehiro Mizusawa [b], Yuji Sakasegawa [f], Kiyotoshi Kaneko [a,*]

[a] *Second Department of Physiology, Tokyo Medical University, Shinjuku-ku, Tokyo 160-8402, Japan*
[b] *Department of Neurology and Neurological Science, Graduate School of Medicine, Tokyo Medical and Dental University, Bunkyo-ku, Tokyo 113-0034, Japan*
[c] *Ultrastructural Research, National Institute of Neuroscience, National Center of Neurology and Psychiatry, Kodaira, Tokyo 187-8502, Japan*
[d] *Department of Neurology and Nephrology, Nippon Medical School, Bunkyo-ku, Tokyo 113-8602, Japan*
[e] *Second Department of Pathology, Nippon Medical School, Bunkyo-ku, Tokyo 113-8602, Japan*
[f] *Division of Prion Protein Biology, Department of Prion Protein Research, Graduate School of Medicine, Tohoku University, Aoba-ku, Sendai 980-8575, Japan*

Received 6 July 2005
Available online 26 September 2005

**Abstract**

We established a histobiochemical approach targeting micron-order inclusion bodies possessing extensive aggregation properties in situ by using a nonchemical denaturant (oligomeric actin interacting protein 2/D-lactate dehydrogenase protein 2 [Aip2p/Dld2p]) with the combinatorial method of laser-microdissection and immunoblot analysis. As a model, pick bodies were chosen and laser-microdissected from three different brain regions of two patients with Pick's disease. Initially, 500 to 2000 pick bodies were applied onto SDS–PAGE gels after boiling in Laemmli's sample buffer according to established immunoblotting procedures; however, only faint signals were obtained. Following negative results with chemical denaturants or detergent, including 6 M guanidine hydrochloride, 8 M urea, and 2% SDS, the laser-microdissected pick bodies were pretreated with oligomeric Aip2p/Dld2p, which possesses robust protein unfolding activity under biological conditions. Strikingly, only one pick body was sufficient to illustrate an immunoblot signal, indicating that pretreatment with oligomeric Aip2p/Dld2p enhanced the immunoblot sensitivity by more than 100-fold. Pretreatment with oligomeric Aip2p/Dld2p also allowed us to quantify the total protein content of pick bodies. Thus, use of oligomeric Aip2p/Dld2p significantly contributed toward the acquisition of information pertaining to the molecular profile of proteins possessing an extensive aggregation property, particularly in small amounts.


*Keywords:* Oligomeric Aip2p/Dld2p; Protein conformation unfolding activity; Laser-microdissection; Inclusion bodies; Pick bodies; Phosphorylated tau

While immunohistochemical analysis has been widely used for the characterization of microstructures under various conditions and of disorders at a light microscopic level, immunoblot analysis has been indispensable in the analysis of proteins at a macroscopic level [1]. Currently, no analytical methods equivalent to the immunoblot have been developed against targets for examination under the microscope, although the recent development of a laser-microdissection methodology allows us to manipulate microstructures at microscopic regions of interest in situ [2].

* Corresponding author. Fax: +81 3 3351 6544.
*E-mail address:* k-kaneko@tokyo-med.ac.jp (K. Kaneko).

0003-2697/$ - see front matter © 2005 Elsevier Inc. All rights reserved.
doi:10.1016/j.ab.2005.09.004

Against this backdrop, we developed a novel combinatorial method that uses laser-microdissection and immunoblotting to allow the characterization of the molecular profile of proteins at microscopic regions of interest. As a model, we examined brain samples of Pick's disease, a type of progressive presenile dementia that affects brain function, eventually causing loss of verbal skills and problem-solving ability [3]. Pick's disease accounts for 5% of all dementias and is characterized neuropathologically by distinct tau-immunoreactive intraneuronal inclusions known as pick bodies [4]. Abnormally phosphorylated tau proteins were detected from total brain homogenates [4–6], but no investigation has been reported with isolated pick bodies to date.

Given limited sample availability and the absence of in vitro amplification steps for proteins, use of laser-microdissected samples depends largely on highly sensitive protein detection methods [7]. Furthermore, these inclusion bodies generally possess extensive aggregation properties that often negatively affect the immunoblot assay. Unfortunately, use of conventional procedures, including sample pretreatment with chemical denaturing agents or detergent, was ineffective. In an effort to overcome the problem, oligomeric actin interacting protein 2 (Aip2p)[1] [8]/D-lactate dehydrogenase protein 2 (Dld2p) [9,10] was used as a nonchemical denaturant [11–13]. Dld2p [9,10] was initially identified as Aip2p using a two-hybrid screen to search for proteins that interact with actin [8]. During our search for protein conformation unfolding activity, we further identified oligomeric Aip2p/Dld2p isolated from *Saccharomyces cerevisiae* as exhibiting robust protein conformation unfolding activity [11]. Oligomeric Aip2p/Dld2p possesses a unique grapple-like structure with an ATP-dependent opening that is required for protein conformation unfolding activity [12,13]. In the presence of 1 mM ATP or AMP–PNP, oligomeric Aip2p/Dld2p bound to all substrates so far examined and subsequently modified the protein conformation. Furthermore, oligomeric Aip2p/Dld2p was able to modify the conformation of pathogenic highly aggregated polypeptides such as recombinant prion protein (rPrP) in the beta form, alpha-synuclein, and Abeta (1–42) in the presence of ATP in vitro [13]. This procedure consists simply of combining oligomeric Aip2p/Dldp2 and 1 mM ATP in a reaction tube containing the collected pick bodies and then incubating the sample for 60 min at 30 °C.

Oligomeric Aip2p/Dld2p significantly increases the immunoblot signals by more than 100-fold. The histobiochemical approach detailed in this study allows us to analyze single pick bodies in the order of several micrometers in radius.

[1] *Abbreviations used:* Aip2p, actin interacting protein 2; Dld2p, D-lactate dehydrogenase protein 2; rPrP, recombinant prion protein; BSA, bovine serum albumin; EGTA, ethyleneglycotetraacetic acid; TCA, trichloroacetic acid; PBS, phosphate-buffered saline; PBS-T, PBS containing 0.05% Tween 20; TBH, total brain homogenate; LC–MS/MS, liquid chromatography–tandem mass spectrometry.

## Materials and methods

After informed consent had been obtained, frontal (Y337F and Y332F) and temporal (Y332T) cortexes from two patients with sporadic Pick's disease (patient 1 (Y337): female, 71 years old; patient 2 (Y332): male, 72 years old) were placed in a deep freezer (−80 °C) at Nippon Medical School until use. The procedures followed were in accordance with the institutional ethical standards on human experimentation.

Oligomeric Aip2p/Dld2p was expressed and purified as described previously [11,12]. Anti-tau AT8 (phosphorylation-dependent monoclonal antibody specific to phosphorylated Ser202/Thr205) and AT100 (specific to phosphorylated Thr212/Ser214) were purchased from Innogenetics. Anti-Aip2p/Dld2p antibody was raised against the synthetic peptide corresponding to the C-terminal 15 amino acid residues of Aip2p (VHYDPNGILNPYKYI) that were coupled through a COOH-terminal cysteine residue to bovine serum albumin (BSA) [11].

Slide preparations were made using a NexES Automated Immunohistochemistry Staining System (Ventana Medical Systems) with 1:200 AT8. Immunostained pick bodies (10–15 μm in diameter) (Table 1) were dissected using a Laser Microdissection System (Olympus Optical) coupled to a Hoya laser cutter (HCL2100, 30 mJ/pulse, 266 nm). Dissected samples were collected using a Cell Tram Oil hydraulic manual microinjector (Eppendorf) with distilled water.

Immunoblot analyses were performed as follows. First, total brain homogenates (10–40 μg) or laser-dissected pick bodies (500 pieces) were solubilized in 500 μl of ice-cold extraction buffer (Tris–chloride [pH 7.4], 0.8 M NaCl, 1 mM ethyleneglycotetraacetic acid [EGTA], 10% sucrose, and 1/1000 [w/v] protease inhibitor cocktail [Sigma] with 1% sodium *N*-lauroyl sarcosinate [sarkosyl]). Sarkosyl-insoluble fractions were collected by centrifugation at 182,000*g* for 30 min at 4 °C and then suspended in 50 mM Tris–chloride (pH 7.4). Samples were pretreated with 8 M urea (Wako Chemicals), 6 M guanidine hydrochloride (Nacalai Tesque), or 2% SDS (Wako Chemicals), followed by trichloroacetic acid (TCA) precipitation in an effort to denature or untangle the samples. Pretreatment with Aip2p/Dld2p was performed as described previously

Table 1
Quantitative analyses of pick bodies

| | Y332T | Y332F | Y337F |
|---|---|---|---|
| Total protein (ng/pick body) | 0.8 | 1.1 | 2.8 |
| Average diameter (μm) | 10 | 10 | 15 |
| SRelative density | 1.6 | 2.2 | 1.6 |

*Note.* The protein concentration of sarkosyl-insoluble fractions was measured following pretreatment with oligomeric Aip2p/Dld2p, and the relative density of the pick bodies was calculated. Frontal (Y337F and Y332F) and temporal (Y332T) cortexes from two patients with sporadic Pick's disease (patient 1 (Y337): female, 71 years old; patient 2 (Y332): male, 72 years old) were analyzed.

[11–13]. Briefly, 1 to 500 ng of oligomeric Aip2p/Dld2p was mixed with the sarkosyl-insoluble fraction of 1 to 500 pick bodies at a ratio of 1 ng per 1 pick body in the presence of 1 mM ATP for 60 min at 30 °C in a total volume of 20 μl. Samples were then loaded onto 12% SDS–PAGE gels and transferred onto 0.22-μm nitrocellulose membranes in 25 mM Tris–190 mM glycine–0.01% SDS–20% methanol at 400 mA for 40 min at 4 °C. Membranes were blocked using 4% BSA in phosphate-buffered saline (PBS) containing 0.05% Tween 20 (PBS-T), incubated with 1:1000 (unless otherwise indicated) AT8 and AT100 in PBS-T overnight at 4 °C, washed with PBS-T several times at room temperature, and then incubated with 1:10,000 horseradish peroxidase-conjugated anti-mouse IgG antibody (Amersham) in PBS-T for 1 h at room temperature. After washing the membranes, the immunodecorated bands were visualized using ECL-plus (Amersham) and then analyzed using a Fluor-S MAX MultiImager or VersaDoc (Bio-Rad Laboratories).

The protein concentration of the pick bodies pretreated with oligomeric Aip2p/Dld2p was measured using a spectrophotometer (Tecan) at 595 nm in combination with a Protein Assay System (Bio-Rad Laboratories) according to the manufacturers' instructions. Oligomeric Aip2p/Dld2p was applied at a ratio of 1 ng per 1 pick body, and the value was subtracted afterward.

## Results

The laser-microdissection system combined with the sample collector facilitated the dissection of targets (Fig. 1A). Up to 500 pick bodies were collected each time over a period of 1 day. Initially, 500 pick bodies were applied onto SDS–PAGE gels after boiling in Laemmli's sample buffer according to established immunoblotting procedures [1]. However, only faint and blurred signals were obtained with anti-tau antibodies AT8 and AT100 (Fig. 1B, lane 4) in comparison with 10 to 40 μg of total brain homogenate (TBH, Fig. 1B, lanes 2 and 3). Immunostaining of the entire gel, including the loading wells and the stacking gel, revealed no additional immunoblot signals that may have arisen from the extensive aggregation property of the pick bodies. Further increases in the number of pick bodies applied (up to 2000) could not improve the signal intensity (data not shown).

The effect of chemical denaturants or detergent, including 6 M guanidine hydrochloride, 8 M urea, and 2% SDS,

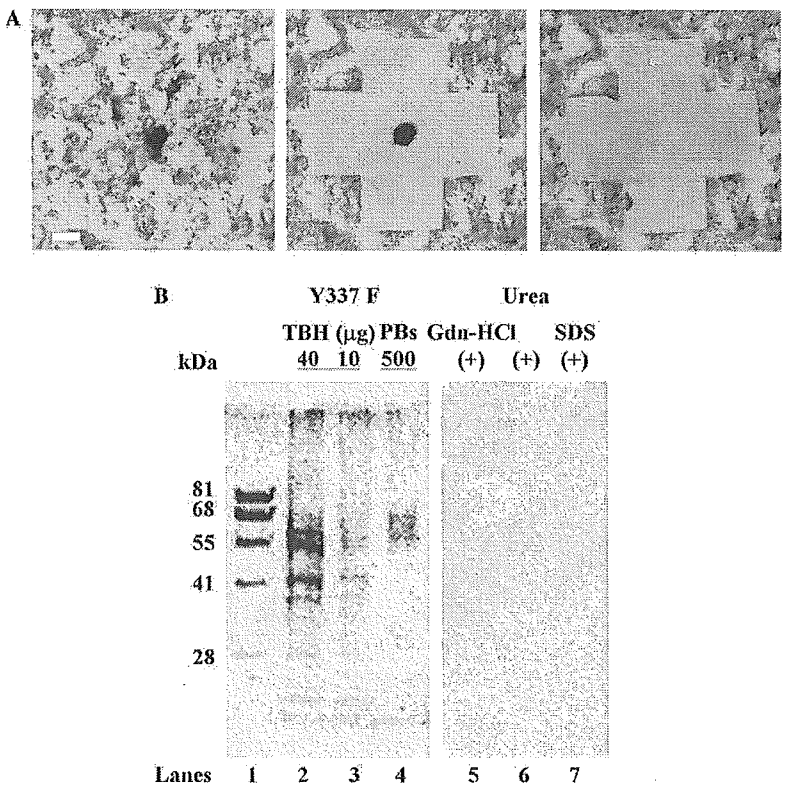


Fig. 1. Immunological analyses of laser-microdissected pick bodies (PBs). (A) Left panel: 5-μm-thick cryosection. PBs of frontal cortex from patient Y337 (Y337F) are stained with AT8 (1:200, purple) and hematoxylin (blue). Middle and right panels: PBs isolated from the section using a laser-microdissector. Scale bar is 10 μm. (For interpretation of the references to color in this figure legend, the reader is referred to the Web version of this article.) (B) Immunoblot analyses of PBs pretreated with chemical denaturants or detergent. Approximately 500 PBs were used for each trial. Lane 1: molecular weight marker (Dr. Western, Oriental Yeast); lanes 2 and 3: total brain homogenate (TBH) of Y337F (40 and 10 μg, respectively); lanes 4 to 7: 500 laser-microdissected PBs of Y337F with no pretreatment (lane 4), 6 M guanidine hydrochloride (Gdn-HCl, lane 5), 8 M urea (lane 6), and 2% SDS pretreatment (lane 7). Samples were stained with anti-tau AT8 (1:1000) and AT100 (1:1000).

was then determined. Use of the aforementioned chaotropic agents, however, resulted in no improvement of immunoblot signals (Fig. 1B, lanes 5–7). In fact, the signal intensities diminished somewhat, possibly due to the presence of phosphorylated tau bound to the walls of the tube after removing the chaotropic agents prior to loading onto the SDS–PAGE gels [14].

Although negative results were obtained following use of the aforementioned chemical denaturants and detergent, we demonstrated that oligomeric Aip2p/Dld2p could modify the conformation of pathogenic highly aggregated polypeptides such as rPrP in the beta form, alpha-synuclein, and Abeta (1–42) in the presence of ATP [13]. Hence, the pick bodies were pretreated with oligomeric Aip2p/Dld2p prior to loading onto SDS–PAGE gels. Surprisingly, immunoblot analyses of Y337F, Y332F, and Y332T demonstrated discrete bands stained with anti-tau AT8 and AT100 antibodies following pretreatment with oligomeric Aip2p/Dld2p (Fig. 2). In a serial dilution assay, 1/500 of 500 pick bodies (equivalent to 1 pick body) was detected (Fig. 2, upper panel, lanes 4–8; lower panel, lanes 2–10).

These immunoreactive bands migrated slightly faster than those associated with the 500 pick bodies processed without oligomeric Aip2p/Dld2p pretreatment (Fig. 2, upper panel, lane 2). One possible explanation is that pretreatment with oligomeric Aip2p/Dld2p might allow the detection of the phosphorylated form of 60 kDa tau (tau 60) [4–6], whereas only the phosphorylated form of 69 kDa tau (tau 69) is negligibly detected following boiling in Laemmli's sample buffer according to classical immunoblotting procedures. Whether the different tau isoform could account for the faster migration pattern observed remains to be determined.

Oligomeric Aip2p/Dld2p was also detected in the same reaction mixtures using anti-Aip2p/Dld2p antibody (Fig. 2, upper panel, lanes 12–16) but did not cross-react with anti-tau AT8 and AT100 antibodies (Fig. 2, upper panel, lane 10). It should be noted that a single pick body directly pretreated with oligomeric Aip2p/Dld2p was sufficient to yield an immunoblot signal (Fig. 2, lower panel, lane 13), indicating that pretreatment with oligomeric Aip2p/Dld2p enhanced the immunoblot signal by more than 100-fold. Transmission electron microscopy with uranyl acetate negative staining of laser-microdissected pick bodies (Fig. 3) revealed that they were untangled following treatment with oligomeric Aip2p/Dld2p, whereas the

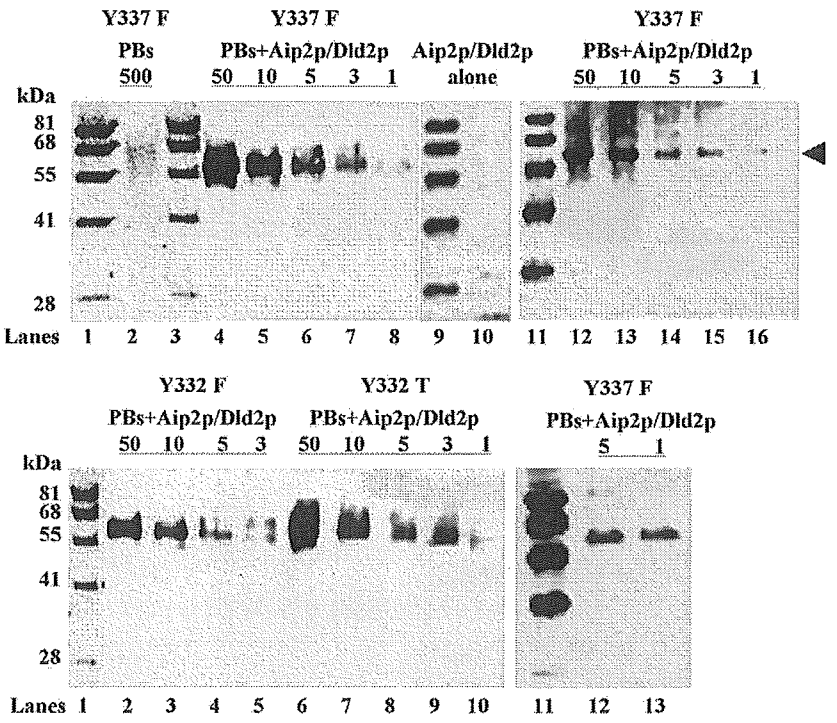


Fig. 2. Immunoblot analyses of laser-microdissected pick bodies (PBs) from Y337F (frontal cortex), Y332F (frontal cortex), and Y332T (temporal cortex). Upper panels: Molecular weight marker (Dr. Western, Oriental Yeast, lanes 1, 3, 9, and 11), 500 laser-microdissected PBs of Y337F (lane 2), and serial dilutions equivalent to 50, 10, 5, and 3 PBs and 1 PB of Y337F (lanes 4–8 and 12–16). Lane 2 represents sample without oligomeric Aip2p/Dld2p pretreatment, whereas lanes 4 to 8 and lanes 12 to 16 represent samples with oligomeric Aip2p/Dld2p pretreatment. Lane 10: 50 ng of Aip2p/Dld2p alone. Lanes 2, 4 to 8, and 10 were stained with anti-tau AT8 (1:1000) and AT100 (1:1000), whereas lanes 12 to 16 were stained with anti-Aip2p/Dld2p polyclonal antibody. The arrowhead indicates the position of Aip2p/Dld2p (MW = 58 kDa). Lower panels: Molecular weight marker (Dr. Western, Oriental Yeast, lanes 1 and 11), serial dilutions of 500 PBs of Y332F equivalent to 50, 10, 5, and 3 PBs (lanes 2–5), and those of Y332T equivalent to 50, 10, 5, and 3 PBs and 1 PB (lanes 6–10). Lanes 12 and 13: 5 PBs and 1 PB of Y337F, respectively. Samples in lower panels were pretreated with oligomeric Aip2p/Dld2p and stained with anti-tau AT8 (1:1000) and AT100 (1:1000).

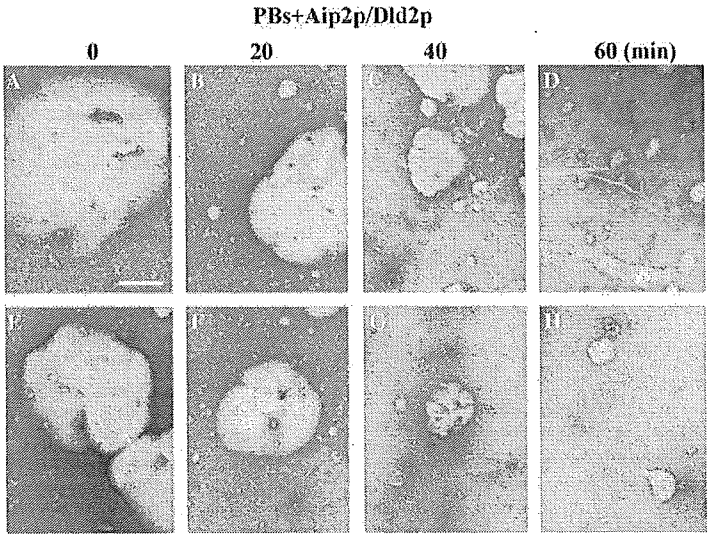


Fig. 3. Transmission electron microscopy with uranyl acetate negative staining of laser-microdissected pick bodies (PBs) prior to (A and E) and following oligomeric Aip2p/Dld2p pretreatment for 20 min (B and F), 40 min (C and G), and 60 min (D and H). For the negative staining, 500 PBs of Y332F were used as specimens. Scale bar is 4 μm.

average diameter of pick bodies decreased markedly, from 10 to 15 μm to less than 1 μm, in a time-dependent manner.

Although protein quantification of highly aggregated proteins such as pick bodies has been quite problematic to date, pretreatment with oligomeric Aip2p/Dld2p allows the ready quantification of the protein content of pick bodies (Table 1). The protein concentrations of sarkosyl-insoluble fractions were 0.8 ng (Y332T), 1.1 ng (Y332F), and 2.8 ng (Y337F) per 1 pick body. Because the average diameters of the pick bodies were 10 μm (Y332) and 15 μm (Y337), the relative densities of the pick bodies were 1.6 to 2.2 (Y332) and 1.6 (Y337).

## Discussion

Our novel combinatorial method targets proteins relating to specific regions of interest at the micrometer order and exclusively allows the gathering of information pertaining to the molecular profile, such as molecular weight, of target proteins under the microscope in situ. During our investigations, we noticed that laser-microdissected pick bodies exhibited only faint and blurred immunoblot signals with anti-tau AT8 and AT100 antibodies, even following pretreatment with chemical denaturants or detergent, presumably resulting from the extensive aggregation property. In fact, this is extremely crucial when only a minimal quantity of target protein is available.

The protein conformation unfolding activity of oligomeric Aip2p/Dld2p can modify the conformation of pathogenic highly aggregated polypeptides [13]. Therefore, pick bodies were pretreated with oligomeric Aip2p/Dld2p to overcome the extensive aggregation property. With the pretreatment, 500 ng of oligomeric Aip2p/Dld2p (MW ~700 kDa) was mixed with 500 pick bodies consisting of abnormally phosphorylated tau (MW = 58 kDa), indicating that the stoichiometry of oligomeric Aip2p/Dld2p:phosphorylated tau is approximately 1:10. As shown in Fig. 2, oligomeric Aip2p/Dld2p pretreatment enhanced the immunoblot signals by more than 100-fold.

The inclusion bodies, which might protect against toxicity [15], have been associated with various protein conformation disorders, including Alzheimer's disease [16], Parkinson's disease [17], and prion disease (e.g., bovine spongiform encephalopathy) [18]. Actually, the robust protein conformation unfolding activity of oligomeric Aip2p/Dld2p modulated the conformation of Abeta (1–42) peptide associated with Alzheimer's disease, alpha-synuclein associated with Parkinson's disease, and rPrP in the beta form associated with prion disease in vitro [13]. Therefore, use of oligomeric Aip2p/Dld2p with our combinatorial method provides significant improvement in the investigation of normal or abnormal microstructures under various conditions and of disorders with extremely enhanced sensitivity.

Making use of this unprecedented property of oligomeric Aip2p/Dld2p may yield further potential applications. For example, a number of proteomic strategies rely on liquid chromatography–tandem mass spectrometry (LC–MS/MS), but sample preparation methods typically involve the use of detergents and chaotropic agents that often interfere with chromatographic separation and/or electrospray ionization [19]. Use of oligomeric Aip2p/Dld2p, however, would not interfere with the LC–MS/MS procedures and might even prove to be ideal for sample pretreatment. Overall, use of oligomeric Aip2p/Dld2p might significantly facilitate nano-scale analysis, which is often hindered by the aggregation property of target proteins present under various analytical conditions, especially when the sample protein is present in minor quantities.

## Acknowledgments

We thank K. Watanabe and K. Takayama for technical assistance. This work was supported by grants from the Ministry of Health, Labor, and Welfare and the Ministry of Education, Culture, Sports, Science, and Technology, Japan, and from the Core Research for Evolutional Science and Technology (CREST) of Japan Science and Technology Agency.

## References

[1] U.K. Laemmli, Cleavage of structural proteins during the assembly of the head of bacteriophage T4, Nature 227 (1970) 680–685.
[2] T. Tanaka, T. Ito, M. Furuta, C. Eguchi, H. Toda, E. Wakabayashi-Takai, K. Kaneko, In situ phage screening: a method for identification of subnanogram tissue components in situ, J. Biol. Chem. 277 (2002) 30382–30387.
[3] S. Hardin, B. Schooley, A story of Pick's disease: a rare form of dementia, J. Neurosci. Nurs. 34 (2002) 117–122.
[4] V. Zhukareva, D. Mann, S. Pickering-Brown, K. Uryu, T. Shuck, K. Shah, M. Grossman, B.L. Miller, C.M. Hulette, S.C. Feinstein, J.Q. Trojanowski, V.M. Lee, Sporadic Pick's disease: a tauopathy characterized by a spectrum of pathological tau isoforms in gray and white matter, Ann. Neurol. 51 (2002) 730–739.
[5] A. Delacourte, N. Sergeant, A. Wattez, D. Gauvreau, Y. Robitaille, Vulnerable neuronal subsets in Alzheimer's and Pick's disease are distinguished by their tau isoform distribution and phosphorylation, Ann. Neurol. 43 (1998) 193–204.
[6] T. Arai, K. Ikeda, H. Akiyama, Y. Shikamoto, K. Tsuchiya, S. Yagishita, T. Beach, J. Rogers, C. Schwab, P.L. McGeer, Distinct isoforms of tau aggregated in neurons and glial cells in brains of patients with Pick's disease, corticobasal degeneration, and progressive supranuclear palsy, Acta Neuropathol. (Berl.) 101 (2001) 167–173.
[7] W. Martinet, V. Abbeloos, N. Van Acker, G.R. De Meyer, A.G. Herman, M.M. Kockx, Western blot analysis of a limited number of cells: a valuable adjunct to proteome analysis of paraffin wax-embedded, alcohol-fixed tissue after laser capture microdissection, J. Pathol. 202 (2004) 382–388.
[8] D.C. Amberg, E. Basart, D. Botstein, Defining protein interactions with yeast actin in vivo, Nat. Struct. Biol. 2 (1995) 28–35.
[9] A. Chelstowska, Z. Liu, Y. Jia, D. Amberg, R.A. Butow, Signalling between mitochondria and the nucleus regulates the expression of a new D-lactate dehydrogenase activity in yeast, Yeast 15 (1999) 1377–1391.
[10] M.J. Flick, S.F. Konieczny, Identification of putative mammalian D-lactate dehydrogenase enzymes, Biochem. Biophys. Res. Commun. 295 (2002) 910–916.
[11] N.S. Hachiya, Y. Sakasegawa, A. Jozuka, S. Tsukita, K. Kaneko, Interaction of D-lactate dehydrogenase protein 2 (Dld2p) with F-actin: Implication for an alternative function of Dld2p, Biochem. Biophys. Res. Commun. 319 (2004) 78–82.
[12] N.S. Hachiya, Y.H.S. Sakasegawa, A. Jozuka, S. Tsukita, K. Kaneko, Oligomeric Aip2p/Dld2p forms a novel grapple-like structure and has an ATP-dependent F-actin conformation modifying activity in vitro, Biochem. Biophys. Res. Commun. 320 (2004) 1271–1276.
[13] N.S. Hachiya, Y.H.S. Sakasegawa, A. Jozuka, S. Tsukita, K. Kaneko, Oligomeric Aip2p/Dld2p modifies the protein conformation of both properly-folded and misfolded substrates in vitro, Biochem. Biophys. Res. Commun. 323 (2004) 339–344.
[14] K. Kaneko, D. Peretz, K.M. Pan, T.C. Blochberger, H. Wille, R. Gabizon, O.H. Griffith, F.E. Cohen, M.A. Baldwin, S.B. Prusiner, Prion protein (PrP) synthetic peptides induce cellular PrP to acquire properties of the scrapie isoform, Proc. Natl. Acad. Sci. USA 92 (1995) 11160–11164.
[15] M. Tanaka, Y.M. Kim, G. Lee, E. Junn, T. Iwatsubo, M.M. Mouradian, Aggresomes formed by alpha-synuclein and synphilin-1 are cytoprotective, J. Biol. Chem. 279 (2004) 4625–4631.
[16] J.W. Lustbader, M. Cirilli, C. Lin, H.W. Xu, K. Takuma, N. Wang, C. Caspersen, X. Chen, S. Pollak, M. Chaney, F. Trinchese, S. Liu, F. Gunn-Moore, L.F. Lue, D.G. Walker, P. Kuppusamy, Z.L. Zewier, O. Arancio, D. Stern, S.S. Yan, H. Wu, ABAD directly links Abeta to mitochondrial toxicity in Alzheimer's disease, Science 304 (2004) 448–452.
[17] J.T. Greenamyre, T.G. Hastings, Parkinson's: divergent causes, convergent mechanisms, Science 304 (2004) 1120–1122.
[18] M.P. Mayer, H. Schroder, S. Rudiger, K. Paal, T. Laufen, B. Bukau, Multistep mechanism of substrate binding determines chaperone activity of Hsp70, Nat. Struct. Biol. 7 (2000) 586–593.
[19] J. Blonder, M.B. Goshe, R.J. Moore, L. Pasa-Tolic, C.D. Masselon, M.S. Lipton, R.D. Smith, Enrichment of integral membrane proteins for proteomic analysis using liquid chromatography–tandem mass spectrometry, J. Proteome Res. 1 (2002) 351–360.

Available online at www.sciencedirect.com
SCIENCE DIRECT®
Neuroscience Letters 394 (2006) 5–8
Neuroscience Letters
www.elsevier.com/locate/neulet

# Acute limbic encephalitis: A new entity?

Yoko Mochizuki [a,*], Toshio Mizutani [a], Eiji Isozaki [b], Toshiyuki Ohtake [b], Yukitoshi Takahashi [c]

[a] *Department of Pathology, Tokyo Metropolitan Neurological Hospital, 2-6-1 Musashidai, Fuchu-shi, Tokyo 183 0042, Japan*
[b] *Department of Neurology, Tokyo Metropolitan Neurological Hospital, Tokyo 183 0042, Japan*
[c] *Department of Pediatrics, National Epilepsy Center, Shizuoka Institute of Epilepsy and Neurological Disorders, Shizuoka 420 8688, Japan*

Received 3 May 2005; received in revised form 15 August 2005; accepted 22 August 2005

**Abstract**

Clinical cases similar to herpes simplex virus (HSV) encephalitis have accumulated in Japan. Detailed examinations have failed to demonstrate HSV infection. Recently, these cases have been named "non-herpetic acute limbic encephalitis". Only a single autopsy case was so far reported in an abstract form, because many cases showed a good prognosis. The case presented here was that following fever, a 59-year-old woman developed disturbance of consciousness and uncontrollable generalized seizures. Brain MRI revealed abnormal signals in the bilateral medial temporal lobe and along the lateral part of the putamen. Autoantibody against the NMDA glutamate receptor (GluR) IgM-ε2 was detected in the serum, and the GluR IgG-δ2 antibody was positive in cerebrospinal fluid. She died 12 days after onset. An autopsy examination revealed scattered foci consisting of neuronal loss, neuronophagia and some perivascular lymphocytic infiltration in the hippocampus and amygdala, but no haemorrhagic necrosis in the brain. HSV-1, -2 and human herpes virus-6 were negative immunohistochemically. We believe that our autopsy case may contribute to understanding the neuropathological background of non-herpetic acute limbic encephalitis.


*Keywords:* Acute encephalitis; Status epilepticus; Autopsy; Non-herpetic acute limbic encephalitis; Herpes simplex encephalitis

Limbic encephalitis is usually considered to be paraneoplastic, occurring subacutely in association with specific neuronal antibodies [2]. Among the cases with reversible acute or subacute non-paraneoplastic limbic encephalitis, voltage-gated potassium channel (VGKC) antibodies have been reported [12]. Autoantibodies against the NMDA glutamate receptor (GluR), which is considered to be related causally to partial seizures [11], were detected in the acute non-herpetic encephalitis [3].

In Japan, acute encephalitis, in which the clinical picture was comparable with that of herpes simplex virus (HSV) encephalitis but where evidence of HSV infection was not demonstrated, has been reported [5]. Recently, these cases have been named "non-herpetic acute limbic encephalitis" as a possible new subgroup of limbic encephalitis [5,9]. It has been proposed that mild infections and immunological process are the cause of this disease from clinical findings and cerebrospinal fluid (CSF) cytokine levels, elevated level of interleukin-6 [5,9] and unelevated level of interferon-γ [1]. Moreover, it has been indicated that acute limbic encephalitis, HSV encephalitis and other acute limbic encephalitis were etiologically interrelated, because cases of limbic encephalitis similar to non-herpetic acute limbic encephalitis were reported [1,9].

Many previously reported cases of non-herpetic acute limbic encephalitis have shown a rather favorable prognosis [1,4,5,7,8,10]. For this reason, only a single autopsy case was so far reported in an abstract form [7]. We believe that this report contributes to understanding the neuropathological background of the acute limbic encephalitis of unknown etiology.

One week after a fever, a 59-year-old woman developed progressive disturbance of consciousness following generalized tonic seizures. The brain computed tomography showed no abnormalities. CSF examinations showed mononuclear cells 10 μl/l, protein 50 mg/dl and glucose 143 mg/dl. The seizures continued, even though multiple anticonvulsants were administered and mechanical ventilation was performed. Eight days after the onset of unconsciousness and seizures, brain magnetic resonance imaging (MRI) with T2-weighted and FLAIR images revealed high signal intensities in the bilateral medial temporal lobes and along the lateral part of the putamen (Fig. 1). She was admitted to our hospital 10 days after the onset of the seizures. She showed marked emaciation and pneumonia complications. Recurrence of generalized tonic seizures

* Corresponding author. Tel.: +81 423 23 5110; fax: +81 423 22 6219.
*E-mail address:* mochi@ica.nihon-u.ne.jp (Y. Mochizuki).

0304-3940/$ – see front matter © 2005 Elsevier Ireland Ltd. All rights reserved.
doi:10.1016/j.neulet.2005.08.070

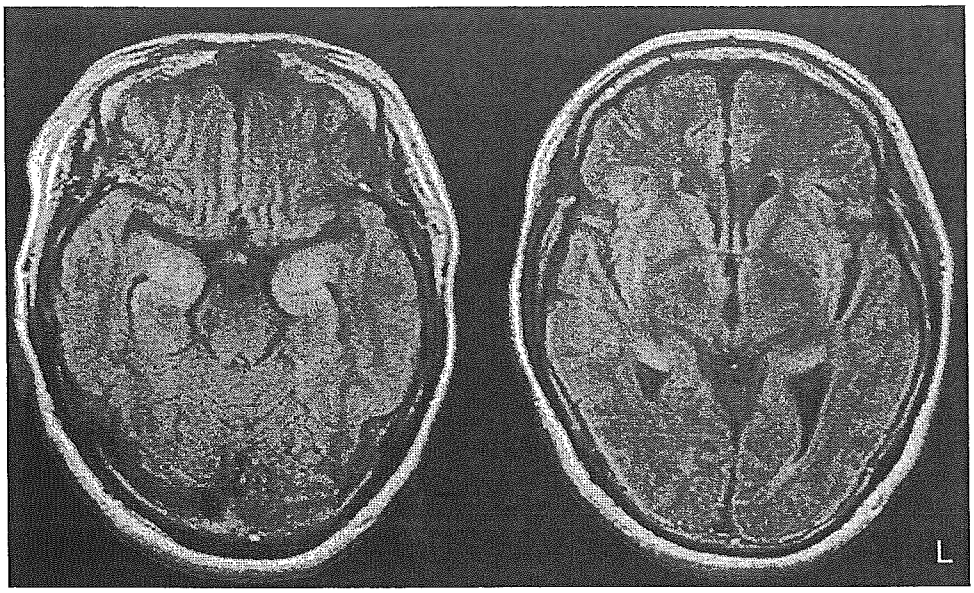


Fig. 1. FLAIR MRI images. High signal intensity is seen in the bilateral medial temporal lobe and the lateral part of the putamen.

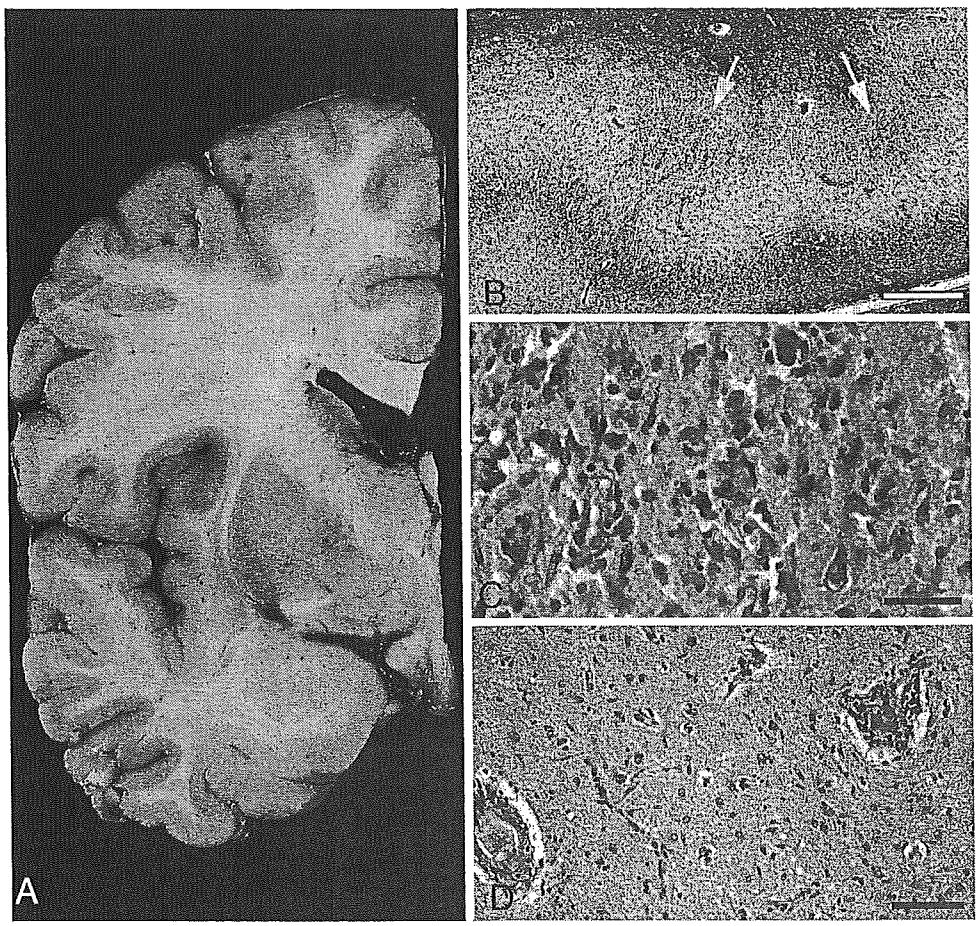


Fig. 2. Neuropathological findings: (A) coronal slice through the left cerebrum. No lesions visible on macroscopic examination; (B) foci of neuronal loss (arrows) surrounded by spongy state in the rostral CA1 of hippocampus. Klüver–Barrera staining (Bar 500 μm); (C) foci of neuronal loss and neuronophagia in the rostral CA1 of hippocampus. Hematoxylin and eosin (HE) staining (Bar 50 μm) and (D) neuronal loss, fibrillary astrocytosis and lymphocytic perivascular cuffing were seen in the rostral part of amygdala. HE staining (bar 50 μm).

failed to be controlled with propofol and acyclovir in addition to the anticonvulsants. An electroencephalogram revealed multifocal spikes without periodic synchronous discharges and periodic lateralized epileptiform discharges. Autoantibodies, including antinuclear antibody, anti-SS-A/B antibodies, and anti-Hu antibodies were all negative. Autoantibody against the GluR IgM-ε2 [11] in the serum was positive, autoantibody against GluR IgG-δ2 in the CSF was positive, and VGKC antibody and P/Q-type voltage-gated calcium channel antibodies were negative in the serum and CSF. Antibodies for several viruses including HSV in the serum and CSF were negative 10 days after the onset of seizures. She had acute renal failure complications and died 12 days after the onset of the seizures.

The direct cause of death was acute renal tubular necrosis and purulent pneumonia. Both laboratory data and pathological examination revealed that the patient did not have any malignant tumors or collagen disease. The brain, weighing 1183 g, was macroscopically unremarkable except for mild swelling (Fig. 2A). Microscopically, there were no leptomeningitis. The amygdala and hippocampus showed small foci of neuronal loss with neuronophagias, proliferation of microglias and hypertrophic astrocytes (Fig. 2B and C). These foci were surrounded by a spongy state. Only a few lymphocytic perivascular cuffings occurred in the amygdala (Fig. 2D). No intranuclear inclusion bodies were found anywhere. Immunohistochemistry for HSV-1, -2 and human herpesvirus-6 was negative. No tissue necrosis or haemorrhage were found in the cerebral cortex including the cingulate, insular, and parahippocampal cortex.

Besides demonstrating evidence of HSV infection, HSV encephalitis shows extensive necrosis with haemorrhage in the medial temporal lobe, insular and cingulate gyri bilaterally [6], where the brain MRI shows high signal intensities. Furthermore, the lesions are bilateral, but not always symmetrical in distribution. In our case, however, abnormal signal intensities were limited in the hippocampus and amygdala bilaterally and symmetrically. No haemorrhagic necrosis was found anywhere, even though there would not have been sufficient time for our patient to develop it. Finally, there were no intranuclear inclusions or immunohistological evidence of HSV infection.

Recently, it is suggested that the presence of autoantibodies against the GluR-ε2 in the CSF of non-herpetic acute encephalitis involves in autoimmune pathogenic mechanism [3,9]. In the CSF of this patient, autoantibody against the GluR-ε2 was negative, while the autoantibody against the GluR-δ2, which is against cerebellar Purkinje cell-specific antibody [11] was positive. The other similar cases as shown in Table 1 [1,4,5,7,8,10] were not examined for the presence of these antibodies. Unfortunately, it remains obscure that this antibody played a role in development of the disease in our case.

There has been only one pathological report of a patient similar to our case: a 53-year-old woman who died 36 days after the onset of illness, and showed neuronal loss in the hippocampus, and neuronophagia and gliosis in the amygdala [7]. As seen in the present patient, this patient showed no evidence of HSV infection, no apparent necrosis in the brain, and the

Table 1
Clinical characteristics and MRI abnormalities of patients with non-herpetic acute limbic encephalitis

| Patients | Kohira et al. [4] | Kusuhara et al. [5] | | | | Asaoka et al. [1] | | | | | | Nonaka et al. [8] | Takahashi et al. [10] | | Maki et al. [7] | Present case |
|---|---|---|---|---|---|---|---|---|---|---|---|---|---|---|---|---|
| | | Case 1 | Case 2 | Case 3 | Case 4 | Case 1 | Case 2 | Case 3 | Case 4 | Case 5 | Case 6 | | Case 1 | Case 2 | | |
| Age (year) | 25 | 40 | 38 | 38 | 53 | 34 | 60 | 73 | 35 | 23 | 18 | 42 | 25 | 58 | 53 | 59 |
| Sex | M | M | F | M | F | M | F | F | M | M | F | F | F | M | F | F |
| Clinical symptoms | | | | | | | | | | | | | | | | |
| Impaired consciousness | 2+ | 3+ | 3+ | + | 3+ | 2+ | + | 2+ | 2+ | 2+ | 2+ | 3+ | + | + | 3+ | 3+ |
| Seizures | 2+ | 2+ | 3+ | + | – | + | + | + | 2+ | + | 3+ | 3+ | 2+ | – | 3+ | 3+ |
| Cerebrospinal fluid | | | | | | | | | | | | | | | | |
| Cells ($mm^3$) | 52 | 17 | 47 | 9 | 10 | 10 | 5 | 32 | 8 | 5 | 320 | 10 | 1 | 76 | normal | 10 |
| Protein(mg/dl) | 25 | 325 | 55 | 27 | 50 | 72 | 32 | 29 | 41 | 28 | 86 | 40 | 15 | 45 | normal | 50 |
| MRI abnormalities | | | | | | | | | | | | | | | | |
| Hippocampi | B | B | B | B | L | B | R>L | B | B | B | L>R | B | B | B | B | B |
| Amygdalae | B | B | B | B | L | B | R>L | B | B | B | L>R | B | B | B | B | B |
| Cingulate gyri | – | – | L | – | – | – | – | B | – | – | – | – | – | – | – | – |
| Sequelae | + | + | + | + | + | + | 2+ | 2+ | + | + | + | + | + | + | died | died |

M: male; F: female; B: bilateral; L: left; R: right, (–): negative; (+): mild; (2+): moderate and (3+): severe.